NEURAL REGENERATION RESEARCH
www.nrronline.org

Research Article

Contribution of ferroptosis and SLC7A11 to light-induced photoreceptor degeneration

Xiaoxu Huang[1, 2, #], Yumeng Zhang[1, 2, #], Yuxin Jiang[1, 2, #], Tong Li[1, 2], Shiqi Yang[1, 2], Yimin Wang[1, 2], Bo Yu[1, 2], Minwen Zhou[1, 2], Guanran Zhang[1, 2], Xiaohuan Zhao[1, 2, *], Junran Sun[1, 2, *], Xiaodong Sun[1, 2]

https://doi.org/10.4103/NRR.NRR-D-23-01741

Date of submission: October 23, 2023

Date of decision: April 27, 2024

Date of acceptance: July 3, 2024

Date of web publication: July 29, 2024

From the Contents

Graphical Abstract

SLC7A11 regulates oxidative stress and ferroptosis in photoreceptors

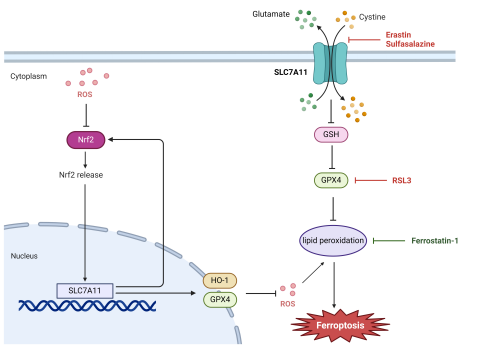

Abstract

Progressive photoreceptor cell death is one of the main pathological features of age-related macular degeneration and eventually leads to vision loss. Ferroptosis has been demonstrated to be associated with retinal degenerative diseases. However, the molecular mechanisms underlying ferroptosis and photoreceptor cell death in age-related macular degeneration remain largely unexplored. Bioinformatics and biochemical analyses in this study revealed xC^-, solute carrier family 7 member 11-regulated ferroptosis as the predominant pathological process of photoreceptor cell degeneration in a light-induced dry age-related macular degeneration mouse model. This process involves the nuclear factor-erythroid factor 2-related factor 2-solute carrier family 7 member 11-glutathione peroxidase 4 signaling pathway, through which cystine depletion, iron ion accumulation, and enhanced lipid peroxidation ultimately lead to photoreceptor cell death and subsequent visual function impairment. We demonstrated that solute carrier family 7 member 11 overexpression blocked this process by inhibiting oxidative stress *in vitro* and *in vivo*. Conversely, solute carrier family 7 member 11 knockdown or the solute carrier family 7 member 11 inhibitor sulfasalazine and ferroptosis-inducing agent erastin aggravated H_2O_2-induced ferroptosis of 661W cells. These findings indicate solute carrier family 7 member 11 may be a potential therapeutic target for patients with retinal degenerative diseases including age-related macular degeneration.

Key Words: age-related macular degeneration; ferroptosis; light exposure damage; oxidative stress; pathway; photoreceptor; programmed cell death; solute carrier family 7 member 11 (SLC7A11)

Introduction

Age-related macular degeneration (AMD), a multifactorial illness, is the most common cause of irreversible and severe visual loss in industrialized nations. One of the main pathological features of AMD is progressive photoreceptor cell death, which results in visual loss with disease progression (Madeira et al., 2015; Lin and Apte, 2018; Deng et al., 2022; Chow and Mead, 2023; Voisin et al., 2023). The molecular processes underlying photoreceptor cell loss in retinal degenerative disorders have not been completely elucidated (Yang et al., 2020). Previous studies on photoreceptor protection have focused on the inhibition of apoptosis (Jaadane et al., 2015; Wu et al., 2020; Xu et al., 2020). However, the incomplete rescue of photoreceptor degeneration by apoptosis inhibitors suggests the involvement of other mechanisms in photoreceptor death (Murakami et al., 2013). Identifying these mechanisms is essential for developing new therapeutic strategies for retinal diseases associated with photoreceptor loss.

Ferroptosis, a form of programmed cell death, is regulated by iron levels and propelled by the buildup of lipid peroxides and the reactive breakdown products, known as lipid-based reactive oxygen species (ROS) (Dixon et al., 2012; Yang and Stockwell, 2016; Pope and Dixon, 2023). The retina is uniquely susceptible to lipid peroxidation owing to its abundance of peroxidation-sensitive polyunsaturated fatty acids and its exposure to a high-energy, oxygen-rich environment (Handa et al., 2017). Disruption in the equilibrium between the retinal oxidation and antioxidant systems enhances the generation of highly reactive molecular species such as ROS and nitrogen free radicals, ultimately resulting in the degeneration of photoreceptors (Brown et al., 2019; Blasiak, 2020; Zou et al., 2022). Previous studies have shown increased iron accumulation in the degenerative retina of multiple animal models (Sun et al., 2018; Ugarte et al., 2018; Tang et al., 2021c). Moreover, intravitreal injection of Fe^{2+} significantly induced oxidative stress and photoreceptor degradation in wild-type mice (Shu et al., 2020). The results of these studies indicate that ferroptosis may be involved in retinal

[1]Department of Ophthalmology, Shanghai General Hospital (Shanghai First People's Hospital), Shanghai Jiao Tong University School of Medicine, Shanghai, China; [2]National Clinical Research Center for Eye Diseases; Shanghai Key Laboratory of Ocular Fundus Diseases; Shanghai Engineering Center for Visual Science and Photomedicine; Shanghai Engineering Center for Precise Diagnosis and Treatment of Eye Diseases, Shanghai, China

*Correspondence to: Junran Sun, MD, emiliesun@sina.com; Xiaohuan Zhao, MD, zhaoxiaohuanleslie@163.com.

https://orcid.org/0000-0003-3678-2780 (Junran Sun); https://orcid.org/0000-0001-9109-7909 (Xiaohuan Zhao)

#These authors contributed equally to this work and share first authorship.

Funding: *This study was supported by the National Natural Science Foundation of China, Nos. 82171076 (to XS) and U22A20311 (to XS), 82101168 (to TL); Shanghai Science and technology Innovation Action Plan, No. 23Y11901300 (to JS); Science and Technology Commission of Shanghai Municipality, No. 21ZR1451500 (to TL); and Shanghai Pujiang Program, No. 22PJ1412200 (to BY).*

How to cite this article: *Huang X, Zhang Y, Jiang Y, Li T, Yang S, Wang Y, Yu B, Zhou M, Zhang G, Zhao X, Sun J, Sun X (2026) Contribution of ferroptosis and SLC7A11 to light-induced photoreceptor degeneration. Neural Regen Res 21(1):406-416.*

degenerative diseases. However, the involvement of ferroptosis in the demise of photoreceptor cells and the specific molecular mechanisms remain uncertain.

As an integral part of the cystine/glutamate transporter system, xC^-, solute carrier family 7 member 11 (SLC7A11) facilitates the uptake of extracellular cystine while releasing intracellular glutamate (Lang et al., 2019). SLC7A11 inhibition results in elevated lipid peroxidation levels and decreased cellular antioxidant capacity, ultimately leading to ferroptosis (Dong et al., 2020). However, the role of SLC7A11 in the development of retinal degenerative diseases, particularly in regulating the redox status and ferroptosis of photoreceptors, has not been explored.

This study investigated the impact of SLC7A11 on ferroptosis using a mouse model subjected to retinal damage induced by light exposure and sodium iodate (NaIO3). We used a murine photoreceptor-derived cell line (661W) to clarify the underlying molecular mechanisms. We also investigated whether SLC7A11-mediated oxidative stress–induced ferroptosis played a role in the progression of retinal degeneration.

Methods

Microarray analysis

We downloaded sequencing data (GSE37773) from Gene Expression Omnibus (GEO) database (https://www.ncbi.nlm.nih.gov/geo/). Data were derived from albino mice exposed to 10,000 lx cool-white fluorescent light for 18 hours; mice were sacrificed at 4 hours after the photic injury, and RNA samples were extracted from the retinas. We used R programming language and Bioconductor packages (http://www.bioconductor.org) for statistical analyses. Differential hybridized features were detected through Bayes-moderated t-statistics with the Bioconductor package "limma" (http://www.bioconductor.org). Genes with *P*-value ≤ 0.05 were defined as significant differentially expressed genes.

Animals and treatment

To establish the model of light-induced retinal degeneration (LIRD), we used C57BL/6 male mice (8–10 weeks old, 18–25 g) provided by GemPharmatech Co., Ltd. (Shanghai, China) (license No. SCXK (Hu) 2023-0009). The mice were raised in specific-pathogen-free (SPF) grade environment with a 12-hour light-dark cycle, an ambient temperature of 22°C and a relative humidity of 40%–70%. Previous studies have successfully used male mice (Kim et al., 2020), female mice (Di Pierdomenico et al., 2020), and both sexes (Natoli et al., 2016) for the LIRD model and no sex differences were reported. In this study, we used male mice for our experiments.

The mice were divided into LIRD-1 day, LIRD-3 day, and control groups (n = 20 mice in each group) using the random number table method. The LIRD-treated groups underwent daily exposure to white LED light provided by a light box (Tow-Int Tech, Shanghai, China) at an intensity of 100K lx for a continuous 8-hour period over 1 and 3 days, following established protocols (Zhang et al., 2022). The control group received treatment under normal conditions (22°C consistent with the light box temperature, and approximately 50 lx ambient light). Detailed information about the experimental design and timeline of the LIRD model is presented in **Additional Figure 1**.

To establish the $NaIO_3$-induced retina degeneration mouse model, mice were divided into five groups with 9 mice in each group. Four groups received intraperitoneal injections of $NaIO_3$ (Sigma, St. Louis, MO, USA) at a dose of 50 mg/kg at different time points (6 hours, 1, 3, and 7 days) as described in a previous study (Chowers et al., 2017). The control group received injections of 100 µL 1×phosphate-buffered saline (PBS). The mice were sacrificed at different time points.

The Animal Research Committee at Shanghai First People's Hospital granted ethical approval for all animal experiments on March 3, 2021 (IACUC number: 2021AWS0142), ensuring rigorous adherence to the guidelines established by the Association for Research in Vision and Ophthalmology for the ethical treatment of animals in ophthalmic and vision research. All animal experiments are reported in accordance with the ARRIVE 2.0 guidelines (Animal Research: Reporting of *In Vivo* Experiments; Percie du Sert et al., 2020).

Virus construction

The experimentally proven Slc7a11-overexpression plasmid was inserted into an adeno-associated virus 2/8 (AAV 2/8) vector (Wang et al., 2014). The recombinant virus was produced together with the control virus rAAV2/8-eGFP in a gene therapy facility (Genomeditech, Shanghai, China) at a titer of 5×10^{12} vg/mL.

Subretinal injection

Mice were anesthetized through intraperitoneal injection of 1.5% sodium pentobarbital (Sigma) at 100 µL/20 g body weight. Prior to the surgical procedure, the pupils were dilated using 1% tropicamid. Under microscopic guidance, a 32-gauge needle was used to puncture the sclera and choroid. A subretinal injection of 2 µL recombinant adeno-associated virus vector (rAAV)2/8-Slc7a11-eGFP (5×10^{12} vg/mL) was administered with a 34-gauge needle connected to a 10 µL microliter syringe at a slow rate. Mice in the control group received subretinal injection of 2 µL rAAV2/8-eGFP. The mice were sacrificed 2 weeks later for the assessment of the transfection efficiency or use in the LIRD model.

Electroretinography

Full-field scotopic electroretinography (ERG) was conducted following established protocols (Zhao et al., 2021b). Briefly, the mice underwent overnight dark adaptation; the next day, mice were anesthetized by intraperitoneal injection of 1.5% sodium pentobarbital under dim red light and both eyes were dilated. A stimulus intensity of 3.0 $cd \cdot s/m^2$ was used to record dark-adapted scotopic a/b-waves using the Ganzfeld flash stimulator (Roland, Brandenburg, Germany).

Immunofluorescence staining

The mice were euthanized by cervical dislocation after anesthesia and eyes were harvested. Eye samples of both eyes were immersed in 4% paraformaldehyde for overnight fixation at 4°C and then dehydrated using 30% sucrose solution for 8 hours. The eyes were then cut into 12 µm lamellar materials with a microtome (Leica, Wetzlar, Germany). Immunofluorescence staining was performed as previously described (Zhao et al., 2021b). The retinal sections were incubated at 4°C overnight with the following primary antibodies: SLC7A11 (rabbit, 1:500, OriGene, Rockville, MD, USA, Cat# TA301518, RRID: AB_2190841), Rhodopsin (mouse, 1:500, Abcam, Cambridge, MA, USA, Cat# ab98887, RRID: AB_10696805), and FITC-labeled Peanut Agglutinin (1:100, XarxBio, Xi'an, China, Cat# R-Y-C-1014-1MG). After three washes in 1×PBS, the sections were incubated with the corresponding secondary antibody at room temperature for 1 hour, followed by DAPI staining (Beyotime, Shanghai, China, Cat# C1002) of nuclei. The sections were examined under a confocal microscope (Leica).

Quantification of nuclei rows

Nuclei rows quantification was performed to ascertain the degree of retinal degeneration as previously described (Di Pierdomenico et al., 2018). Briefly, retinal sections stained with hematoxylin and eosin (H&E, Beyotime) were selected and the numbers of nuclei rows in the outer nuclear layer (ONL) were evaluated at eccentric distances from the optic nerve. Defining the total length of hemi-retina as 100%, the 25%, 50%, 75%, and 95% positions were selected for the calculation. The number of nuclei rows was manually quantified and the measurements were taken three times.

Terminal deoxynucleotidyl transferase-mediated dUTP nick-end labeling assay, propidium iodide staining, and dihydroethidium staining

The *in situ* terminal deoxynucleotidyl transferase-mediated dUTP nick-end labeling (TUNEL) staining for analyzing cell death was performed on retinal sections prepared as described previously (Wang et al., 2021). The experiments were conducted using the TUNEL kit (Roche, Basel, Switzerland) following the manufacturer's instructions. Briefly, after fixation and permeabilization, the retinal sections were stained with 50 µL TUNEL reaction mixture for 1 hour at 37°C in the dark and then photographed using a confocal microscope (Leica). Propidium iodide (PI) (Sigma) staining of the retinal sections was performed following the established protocol. In short, following fixation, the retinal sections were stained with PI at 30 µM for 30 minutes (Zhang et al., 2022), followed by fluorescence microscopy (Leica).

Dihydroethidium (DHE) staining (Beyotime) was used to evaluate ROS levels as previously described (Zhang et al., 2022). The retina sections were stained with DHE at the final concentration of 5 µM for 30 minutes at 37°C and then photographed with a confocal microscope. Nuclei were stained with DAPI (Beyotime).

Cell culture

The murine photoreceptor-derived cell line 661W (RRID: CVCL_6240) was provided by the Department of Ophthalmology of Tongji Hospital, Tongji University School of Medicine, Shanghai, China (Wu et al., 2021). Cells were cultured in Dulbecco's modified Eagle's medium (HyClone, Logan, UT, USA) containing 10% fetal bovine serum (Sigma) and 1% penicillin/streptomycin (Life Technologies, Gaithersburg, MD, USA). The cells were incubated at 37°C in a 95% humidity atmosphere of 5% CO_2 and passaged every 2 to 3 days. The cells were seeded into 6-, 24-, or 96-well plates and incubated overnight.

In experiments, cells were stimulated using different concentrations (200–800 μM) of H_2O_2 (Sigma) for different times (0–24 hours). To examine the mechanisms involved in ferroptosis, we treated the cells with the SLC7A11 inhibitor sulfasalazine (SAS, 400 μM, Sigma), ferroptosis inhibitor ferrostatin-1 (Fer-1, 40 μM, Sigma), and ferroptosis inducer erastin (10 μM, Sigma) or RSL3 (10 μM, Cayman, Ann Arbor, MI, USA), followed by 400 μM H_2O_2 for 24 hours following the experimental design. Detailed information on the 661W cell experimental design and timeline is provided in **Additional Figure 1**.

Lipid peroxidation detection

The BODIPY-C11 581/591 probe (Thermo Fisher Scientific, Waltham, MA, USA) was used to evaluate lipid ROS levels in 661W cells following the previously reported methods (Sun et al., 2018). Cells were incubated in BODIPY-C11 at 2 μM for 30 minutes, harvested using trypsin, and washed three times with PBS. The lipid ROS levels were examined using a fluorescence microscope and determined as the ratio of oxidized (green) to non-oxidized (red) state immunofluorescence intensity.

Iron assay and malondialdehyde determination

Fe^{2+} and total Fe were identified using an iron assay kit (Sigma), and malondialdehyde (MDA) was determined using an MDA assay kit (Beyotime) as described previously (Zhao et al., 2021b). Absorbance was quantified at 595 nm and 535 nm, respectively, with a microplate reader (Tecan, Männedorf, Switzerland).

Glutathione determination

Intracellular glutathione (GSH) in 661W photoreceptor cells incubated with SAS (100–400 μM) was detected using a GSH Assay Kit (Beyotime). A microplate reader was used to measure the absorbance at 405 nm following the provided instructions. The GSH values were determined through a standard curve and calculated as fold change compared with the control group.

Cell viability assays

The 661W cells were plated in 96-well plates and cultured overnight. Cells were then washed by PBS and incubated with Cell Counting Kit-8 reagent (CCK-8, Beyotime) at a ratio of 1:10. After 1–4 hours, the optical densities were detected at 450 nm with a microplate reader.

SLC7A11 RNA interference and overexpression

To explore the specific mechanism of SLC7A11 in ferroptosis, three sequences were synthesized for Slc7a11 siRNAs (siSlc7a11/scramble) by Genomeditech, and the Slc7a11 plasmid (AAV-Slc7a11/vector) was constructed by Genomeditech and verified by DNA sequencing. The 661W cells were transfected with siSlc7a11/scramble or AAV-Slc7a11/vector for at least 24 hours with Lipofectamine 3000 (Invitrogen, Carlsbad, CA, USA), following the manufacturer's instructions. The knockdown and overexpression effects were assessed by western blot and qRT-PCR analysis after 48 hours of transfection. The sequences of siRNAs and AAV-Slc7a11 are listed in **Additional Table 1**.

Flow cytometry analysis

Flow cytometry analysis was performed to quantitatively determine the transfection efficiency. An siRNA labeled with Cy3 and plasmid DNA labeled with ZsGreen were transfected into 661W cells. After over 24 hours of transfection, cells were trypsinized and resuspended in 1 mL PBS. The transfection efficiency was detected using flow cytometry. Cy3 excited with green laser (550 nm) and ZsGreen excited with blue laser (488 nm) were assessed by fluorescence intensity with flow cytometry (Beckman Coulter, Miami, FL, USA).

Western blot analysis

Mouse retinas and 661W cells were lysed in RIPA buffer (Beyotime) and protein concentrations were measured by BCA assays (Pierce, Rockford, IL, USA). Proteins were separated by 4%–20% sodium dodecyl–sulfate polyacrylamide gels and transferred to polyvinylidene fluoride membranes (Millipore, Billerica, CA, USA). After incubation in 5% skim milk at room temperature for 1 hour, the membranes were incubated with primary antibodies overnight at 4°C, followed by incubation with peroxidase-conjugated secondary antibody for 1 hour at room temperature. The bands were detected with ECL reagents (Millipore) using the Amersham Imager 600 imaging instrument (GE Healthcare, Buckinghamshire, UK). Relative protein expression was normalized to β-actin and quantitatively analyzed by ImageJ (X64) software (NIH, Bethesda, MD, USA). The antibodies are listed in **Additional Table 2**.

Quantitative reverse transcription–polymerase chain reaction

Total RNA from mouse retinas and 661W cells was extracted using an RNA simple Total Kit (Tiangen Biotech, Shanghai, China) and cDNA was synthesized using a reverse transcription kit (Takara Bio, Dalian, China) following the manufacturers' instructions. Quantitative reverse transcription–polymerase chain reaction (qRT-PCR) was performed using the following conditions: denaturation at 95°C for 30 seconds, followed by 40 cycles of 95°C for 5 seconds and 60°C for 30 seconds. The relative mRNA expression of the genes was normalized to β-actin gene expression using the ΔCt method ($2^{-\Delta\Delta Ct}$). The primer sequences are listed in **Additional Table 1**.

Statistical analysis

All statistical analyses were performed using GraphPad Prism, version 9.0 (GraphPad Software, San Diego, CA, USA, www.graphpad.com). Data are presented as means ± standard deviation (SD). We used unpaired Student's *t*-tests to compare the statistical results between two groups, while one-way analysis of variance was used to evaluate significant differences among multiple groups. For *post hoc* tests, Tukey's test was performed for pairwise comparison among multi-groups, and the Dunnett's test was applied to evaluate the data from each experimental group compared with the control group. A *P*-value < 0.05 indicated statistical significance.

Results

Light damage increases photoreceptor death

To evaluate photoreceptor cell death in the LIRD mouse model, PI and TUNEL staining was performed on retinal sections. Compared with the control group, the LIRD group had a higher number of PI-positive ($P = 0.0002$) and TUNEL-positive ($P < 0.0001$) cells in the retina in a time-dependent manner (**Figure 1A–C**). Furthermore, the numbers of nuclei rows in the ONL were significantly reduced compared with those in controls, as a result of photoreceptor mortality and loss during LIRD ($P < 0.0001$; **Additional Figure 2**). Excess Fe^{2+}, which is highly cytotoxic through the Fenton reaction, facilitates ferroptotic cell death (Zhao et al., 2021b). The Fe^{2+} concentration ($P = 0.0166$) and proportion ($P = 0.0226$) in the retina significantly increased after 3 days of light exposure (**Figure 1D**), suggesting the involvement of Fe^{2+} in light-induced photoreceptor cell death.

ERG was performed to further assess the changes in retinal function after LIRD. The results showed a significant decrease of a-wave ($P = 0.0010$) and b-wave ($P = 0.0398$) amplitudes 3 days after LIRD (**Figure 1E** and **F**), which indicated light damage to the retina. The pathological changes in retinal structure matched the functional changes suggested by ERG, demonstrating retinal damage in the LIRD model.

Retinal SLC7A11 levels are increased in the LIRD mouse model

To explore the mechanism of photoreceptor death, we performed differential expression analysis using the GSE37773 dataset from the GEO database revealed that the albino mice in LIRD group displayed upregulation of 232 genes and downregulation of 45 genes compared with the control group (log fold-change (|LogFC|) > 2 or < 0.5 and $P < 0.05$). A heatmap of gene expression patterns after light damage is shown in **Figure 2A**. The results revealed upregulation of SLC7A11 and iron metabolic–related proteins such as heme oxygenase (decycling) 1 (Homx1), lipocalin 2 (Lcn2), and transferrin (Trf) in the LIRD group. SLC7A11 showed upregulation with an FC of 3.60 (**Figure 2B**). SLC7A11 expression was also higher in the LIRD group in the database ($P < 0.0001$; **Figure 2C**).

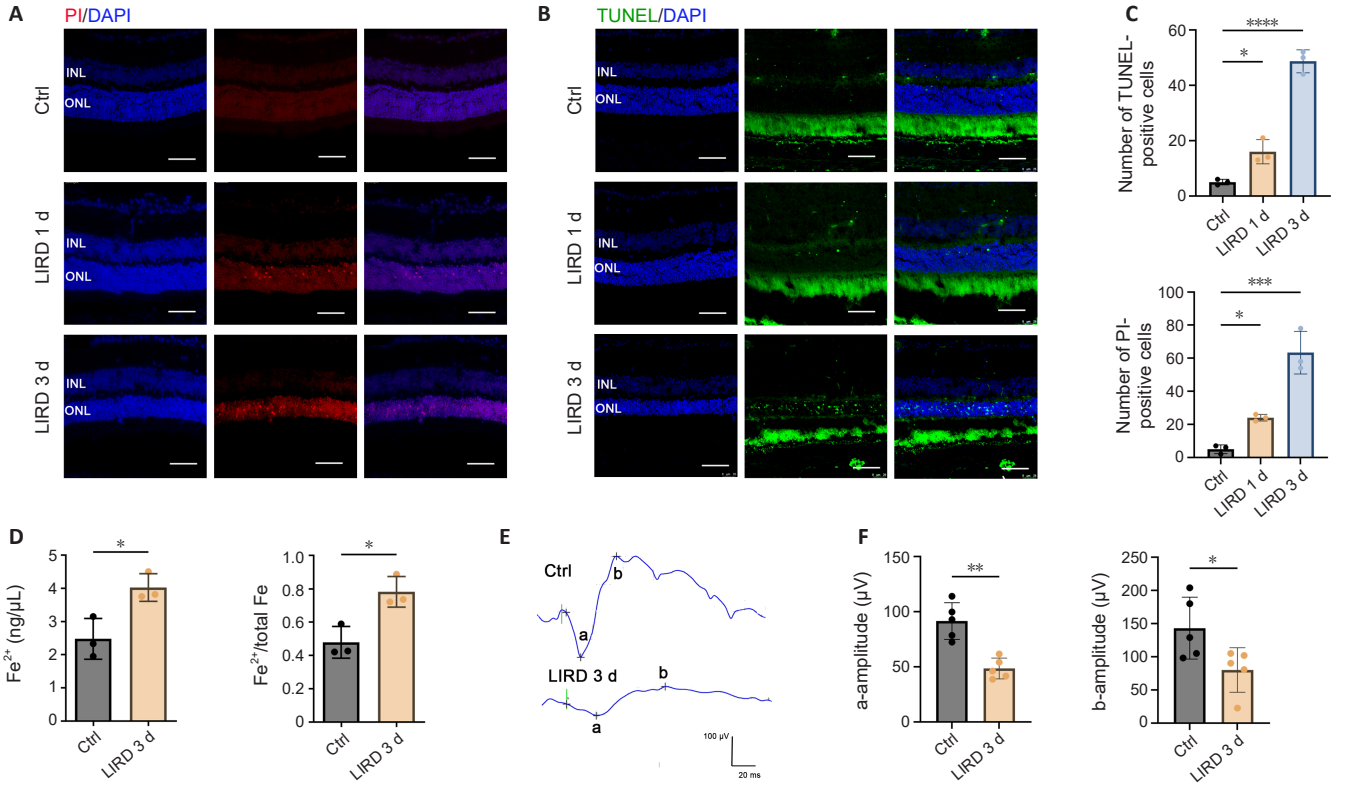

Figure 1 | LIRD induced an increase in photoreceptor death in mice.

(A–C) Cell death tests revealed an increase in PI-positive cells (red) and TUNEL-positive cells (green) in retinal cryosections after LIRD compared with the control group. Nuclei were stained with DAPI (blue) (n = 3). Scale bars: 50 μm. (D) The concentration of Fe^{2+} and Fe^{2+}/total Fe in the retina increased after 3 days of LIRD (n = 3). (E, F) Both the a-wave and b-wave of ERG recordings decreased after 3 days of LIRD compared with 0 day (n = 5). Data in (F) are shown as mean ± SD. *P < 0.05, **P < 0.01, ***P < 0.001, ****P < 0.0001. All experiments were conducted in triplicate. Ctrl: Control; DAPI: 4′,6-diamidino-2-phenylindole; INL: inner nuclear layer; LIRD: light-induced retinal damage; ONL: outer nuclear layer; PI: propidium iodide; TUNEL: terminal deoxynucleotidyl transferase-mediated dUTP nick-end labeling.

To examine the expression levels of SLC7A11 in the LIRD model, we collected retinas from the LIRD group at different time points and performed western blot analysis. SLC7A11 levels increased significantly on day 1 and then decreased on day 3 (P = 0.0038; **Figure 2D** and **E**). RT-PCR analysis also showed upregulated SLC7A11 mRNA levels on day 1, followed by a decline (P = 0.0003; **Figure 2F**). Immunofluorescence showed increased SLC7A11 expression in the ONL of the retina and SLC7A11 localization on the cones and rods on day 1 after LIRD (**Figure 2G** and **H** and **Additional Figure 3**).

Light damage induces ferroptosis and oxidative stress *in vivo*

ROS accumulation in response to adverse external stimuli exceeds the scavenging capacity of the peroxidase system, leading to oxidative stress, triggering lipid peroxidation and, eventually, ferroptosis. We next used DHE staining to measure the ROS levels in mouse retinas with or without light exposure. The ROS levels increased on days 1 and 3 after light exposure, consistent with the change in nuclei rows in the ONL (**Figure 3A**). We measured the levels of several molecules involved in oxidative stress, including nuclear erythroid factor 2-related factor 2 (Nrf2) (P < 0.0001) and heme oxygenase-1 (HO-1) (P = 0.0037) and the levels of these molecules increased after LIRD, peaking on day 3 (P < 0.01; **Figure 3B** and **C**), suggesting the involvement of oxidative stress in light-induced photoreceptor damage. As a negative regulator of ferroptosis, glutathione peroxidase 4 (GPX4) plays a role in reducing lipid hydroperoxide levels. We also observed downregulation of GPX4 after light exposure in a time-dependent manner (P = 0.0012; **Figure 3B** and **C**).

Intraperitoneal injection of NaIO3 is widely used to establish a model of oxidative stress damage (Chan et al., 2019). We next investigated the association of oxidative stress with ferroptosis using this model. Nrf2 and SLC7A11 expression increased 6 hours after NaIO3 treatment, plateaued on day 1 (P < 0.0001), and then decreased, whereas HO-1 expression plateaued on day 3 and then declined (P < 0.0001; **Figure 3D** and **E**). GPX4 expression decreased continuously from days 6 to 7 after treatment (P = 0.0003).

To further investigate the role of SLC7A11 in photoreceptor degeneration, SAS, a pharmacological inhibitor of SLC7A11, was injected intraperitoneally into mice for 3 consecutive days before light exposure. SAS treatment resulted in downregulated expressions of Nrf1, GPX4, and HO-1 (**Figure 3F**) and increased numbers of TUNEL-positive cells in the photoreceptors (**Figure 3G** and **H**).

H_2O_2 treatment causes upregulated SLC7A11 expression and the SLC7A11 inhibitor sulfasalazine promotes ferroptosis in 661W cells

To explore the mechanism of SLC7A11 in photoreceptors, we used 661W cells. After treatment with H_2O_2, BODIPY-C11 581/591 staining showed that lipid peroxidation in 661W cells significantly increased, which was observed as an increase in the ratio of the immunofluorescence intensity of the oxidized/non-oxidized state (P = 0.0019; **Figure 4A** and **B**). To examine the activation of ferroptosis and the increase of lipid peroxidation level, malondialdehyde (MDA) levels were measured in 661W cells with and without H_2O_2 (400 μM) stimulation. The level of MDA in cells of H_2O_2 group was significantly increased compared with the control group (P < 0.01; **Additional Figure 4**).

Subsequently, to investigate the relationship between oxidative stress and SLC7A11 *in vitro*, we treated 661W cells with H_2O_2 at different concentrations and times and analyzed SLC7A11 expression by western blot. We observed significantly up-regulated SLC7A11 expression after H_2O_2 treatment (P = 0.0002; **Figure 4C–F**). The expression of SLC7A11 reached the maximum at the H_2O_2 concentration of 400 μM. **Figure 4E** shows results after different time points of H_2O_2 stimulation, that is, SLC7A11 protein expression increased in a time-dependent manner.

We next explored the potential role of SLC7A11 in photoreceptor degeneration by treating 661W cells with SAS. A previous study showed that SLC7A11 reduces lipid peroxidation in cells to inhibit ferroptosis by transporting cysteine into the cytosol to promote GSH production (Fang et al., 2020). We observed a decrease in GSH level after treatment with 200 μM SAS and GSH level was nearly undetectable following treatment with 400 μM SAS (P < 0.0001; **Figure 4G**). To examine the mechanism of GSH reduction, we examined the levels of enzymes related to GSH synthesis in

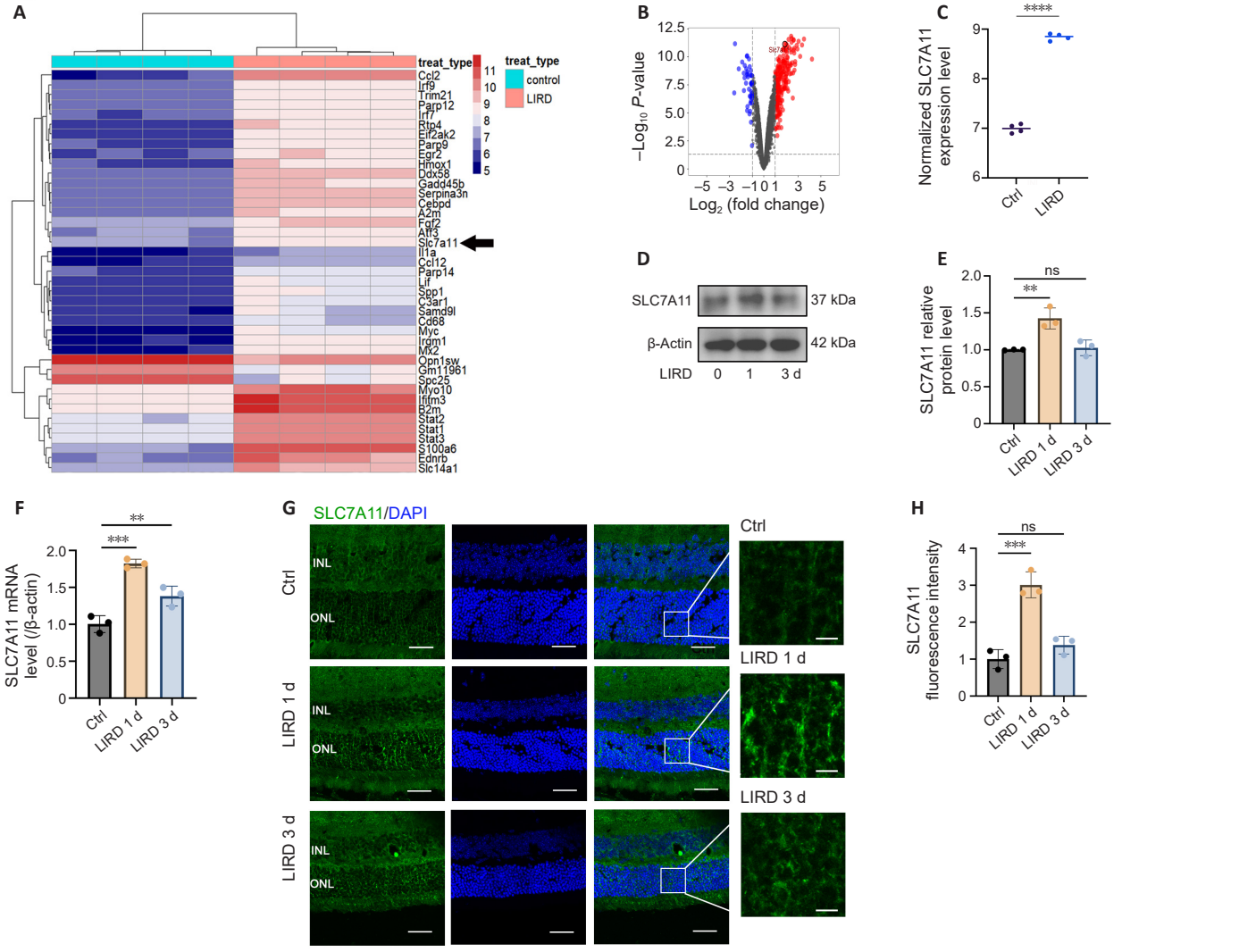

Figure 2 | **The expression of SLC7A11 increases in the retina of LIRD mice.**

(A) Hierarchical clustering analysis of the DEGs between the Ctrl group and LIRD group. (B) Volcano plot of the DEGs (|LogFC| > 1 and $P < 0.05$). (C) SLC7A11 expression in the LIRD group was significantly higher than that in the Ctrl group in the GEO database. (D, E) Western blot showing the protein levels of SLC7A11 in the retina increased after LIRD ($n = 3$). (F) SLC7A11 mRNA levels in the retina increased at day 1 after LIRD ($n = 3$). (G, H) Retinal sections from the LIRD group and control group stained with anti-SLC7A11 (green). Data in H are shown as mean ± SD. $^{**}P < 0.01$, $^{***}P < 0.001$, $^{****}P < 0.0001$. Scale bars: 25 μm for original images, 5 μm for enlarged images. All experiments were conducted in triplicate. Ctrl: Control; DAPI: 4′,6-diamidino-2-phenylindole; DEGs: differentially expressed genes; INL: inner nuclear layer; LIRD: light-induced retinal damage; ns: not significant; ONL: outer nuclear layer; SLC7A11: solute carrier family 7 member 11.

661W cells treated with SAS (**Additional Figure 5A** and **B**). Both glutathione reductase (GR) and glutathione synthase (GS) protein levels showed a SAS concentration–dependent decreasing trend, which was consistent with the change trend of GSH levels after SAS treatment. CCK-8 assay showed that 0–400 μM SAS alone had no effects on 661W cell viability (**Figure 4H**), while SAS combined with H_2O_2 treatment led to decreased cell viability in a dose-dependent manner ($P < 0.0001$; **Figure 4I**).

We next examined ferroptosis-related molecules in the oxidative stress model induced by $NaIO_3$. As a result, the levels of SLC7A11, NRF2 and HO-1 increased and the expression of GPX4 decreased, indicating the induction of ferroptosis during oxidative stress-induced photoreceptor death (**Additional Figure 6**). SAS treatment significantly inhibited the expression levels of GPX4 ($P = 0.0017$), Nrf2 ($P = 0.0001$), and HO-1 ($P = 0.0038$) protein (**Figure 4J** and **K**), which indicated that SLC7A11 inhibition enhanced lipid peroxidation and promoted ferroptosis in 661W cells.

SLC7A11 knockdown increases ferroptosis and SLC7A11 overexpression enhances ferroptosis resistance

To investigate the role of SLC7A11 in photoreceptor ferroptosis, we used Slc7A11 siRNA and overexpression plasmids. Knockdown of Slc7a11 in 661W cells using three target Slc7a11 siRNAs with different sequences (si-Slc7a11#1, #2, and #3) showed that both si-Slc7a11#1 and #3 efficiently knocked down SLC7A11 protein expression (**Figure 5A**). qRT-PCR analysis showed that siSLC7A11#3 exhibited maximum knockdown efficiency of SLC7A11 mRNA ($P = 0.0002$; **Figure 5B**). Thus, si-Slc7a11#3 was selected for subsequent experiments. We did not observe a significant change in for 661W cell viability after siSLC7A11 transfection. To confirm transfection efficiency, we evaluated the transfection of Cy3-labeled siRNA (**Additional Figure 7A–D**). More than 71% of 661W cells were successfully transfected with Cy3-labeled siRNA compared with the cells in control group. Knocking down SLC7A11 significantly decreased the expression of GPX4 ($P = 0.0002$), Nrf2 ($P = 0.0008$), and HO-1 ($P = 0.0108$) after H_2O_2 treatment (H_2O_2 + siRNA group compared with H_2O_2 group) (**Figure 5C** and **D**).

Fer-1 is a potent inhibitor of ferroptosis (Miotto et al., 2020). Fer-1 alone at various concentrations did not significantly affect the viability of 661W cells (**Figure 5E**). From these results, we selected 40 μM for subsequent experiments. CCK-8 assay showed that Fer-1 rescued the reduced cell viability after SLC7A11 knockdown and H_2O_2 exposure (Fer-1 + H_2O_2 + siRNA group compared with H_2O_2 + siRNA group) ($P < 0.0001$; **Figure 5F**), providing further evidence that SLC7A11 knockdown promoted ferroptosis in 661W cells.

We next used the SLC7A11 overexpression plasmid in 661W cells to upregulate SLC7A11 expression. There was no significant change in cell viability after transfecting the SLC7A11-overexpression plasmid into 661W cells. To evaluate the transfection efficiency, we used ZsGreen-labeled plasmid

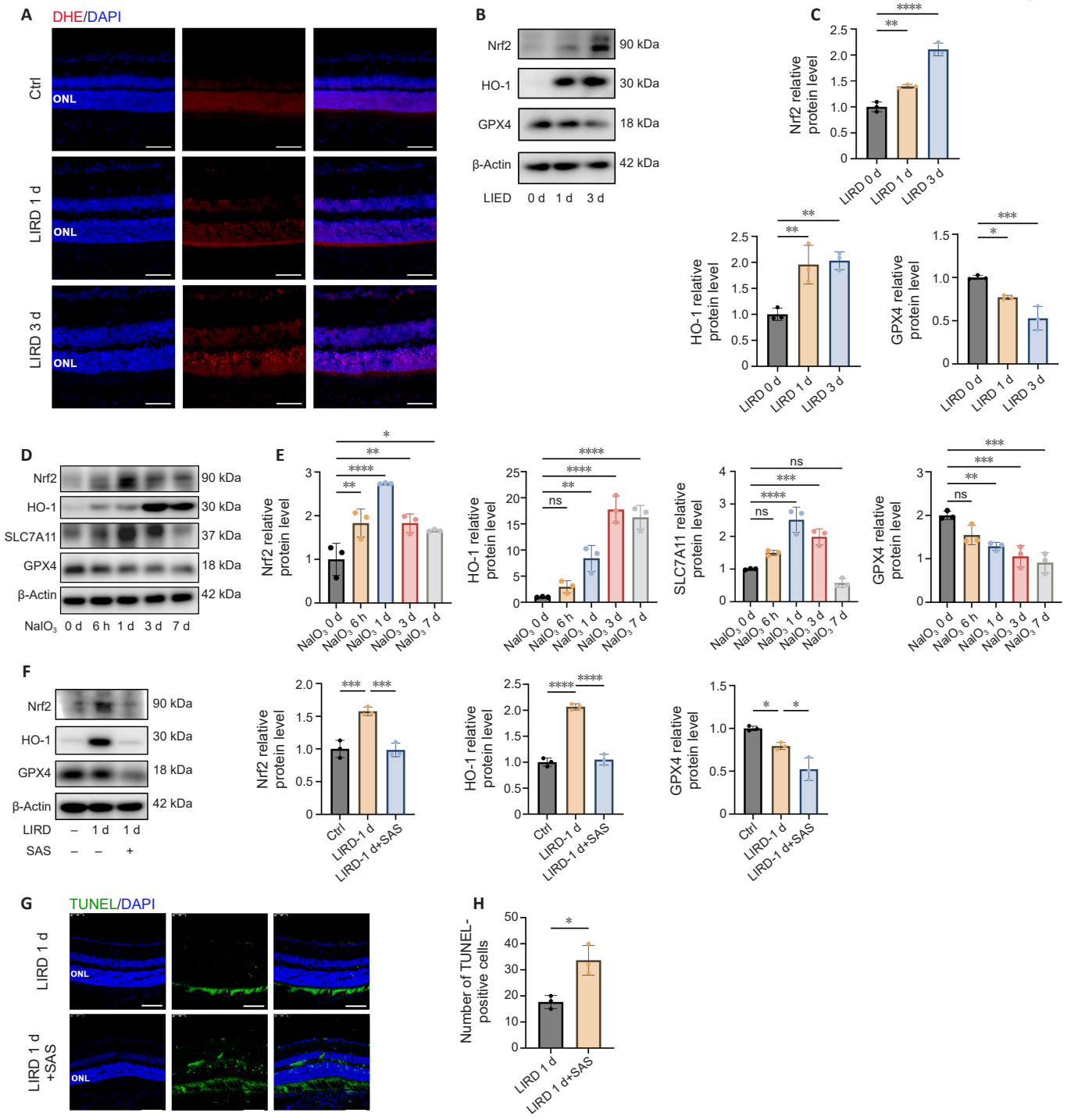

Figure 3 | **Ferroptosis and oxidative stress is induced in response to light damage *in vivo*.**
(A) DHE staining (red) showing a time-dependent increase in ROS levels from 0 to 3 days after LIRD. (B, C) Western blot analysis and data quantification showed that the expression levels of Nrf2, HO-1, and GPX4 in mouse retina were significantly elevated after LIRD (n = 3). (D, E) Western blot showing the expression levels of protein Nrf2, HO-1, SLC7A11, and GPX4 in mouse retina after NaIO3 treatment (n = 3). (F) Western blot showed that pre-treatment of sulfasalazine (SAS, a SLC7A11 inhibitor; 8 mg/kg) before LIRD reduced the expression of Nrf2, HO-1, and GPX4 proteins compared with levels in the LIRD group. (G, H) Cell death in ONL after SAS treatment and LIRD. TUNEL immunoreactivity (green) was increased in retinal sections of SAS-treated LIRD mice compared with the LIRD group (n = 3). Data are shown as mean ± SD. *P < 0.05, **P < 0.01, ***P < 0.001, ****P < 0.0001. Scale bars: 50 μm. All experiments were conducted in triplicate. Ctrl: Control; DAPI: 4′,6-diamidino-2-phenylindole; DHE: dihydroethidium; GPX4: glutathione peroxidase 4; HO-1: heme oxygenase-1; LIRD: light-induced retinal damage; NRF2: nuclear factor-erythroid factor 2-related factor 2; ONL: outer nuclear layer; SAS: sulfasalazine; TUNEL: terminal deoxynucleotidyl transferase-mediated dUTP nick-end labeling.

(**Additional Figure 7E–H**). More than 79% of 661W cells were successfully transfected with ZsGreen-labeled plasmid compared with the cells in control group. Western blotting showed that SLC7A11 overexpression increased SLC7A11, GPX4, Nrf2, and HO-1 expression (**Figure 6A** and **B**), inhibited the H_2O_2-induced downregulation of GPX4 expression and further enhanced levels of anti-oxidant proteins (Nrf2 and HO-1) (**Figure 6C** and **D**).

Erastin, similar to the GPX4 inhibitor RSL3, induces ferroptosis (Chen et al., 2021). CCK-8 assay results showed a dose-dependent reduction in the viability of cells treated with erastin or RSL3 (P < 0.0001; **Figure 6E** and **F**). SLC7A11 overexpression alleviated the decreased cell viability caused by erastin or RSL3 after H_2O_2 exposure (erastin/RSL3 + H_2O_2 + oeSlc7a11 group compared with H_2O_2 + oeSlc7a11 group) (P < 0.0001; **Figure 6G** and **H**). These results demonstrated that SLC7A11 overexpression reduced photoreceptor ferroptosis *in vitro*.

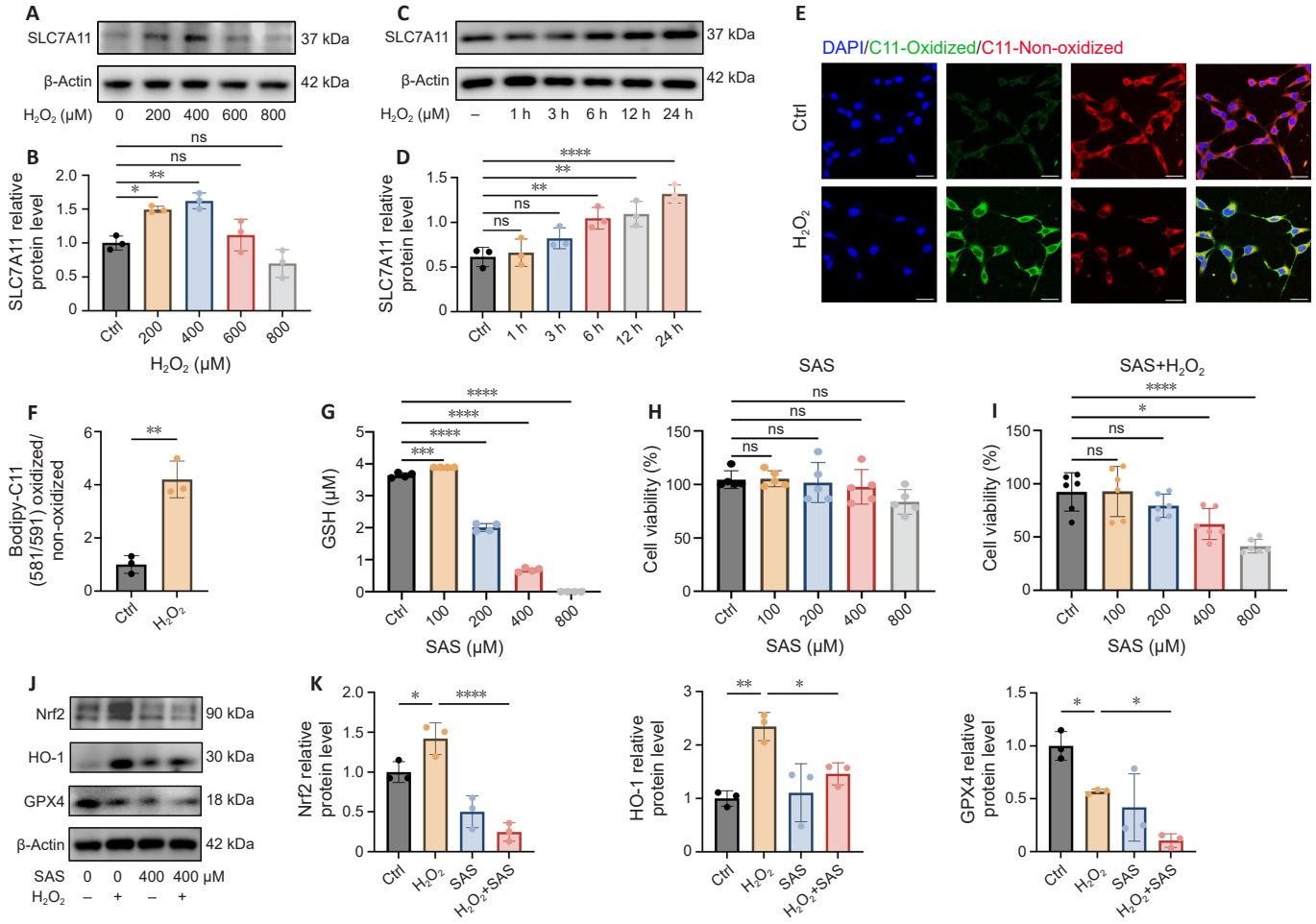

Figure 4 | **SLC7A11 expression was upregulated in 661W cells with H_2O_2-treatment and the SLC7A11 inhibitor SAS promoted 661W ferroptosis.**
(A–D) Western blot showing SLC7A11 protein levels in 661w cells with H_2O_2 treatment at different concentration and time (n = 3). (E, F) The BODIPY TM581/591 staining showed the increased lipid peroxidation level after H_2O_2 treatment (n = 3). Scale bars: 25 μm. (G) The GSH level of 661W cells significantly decreased after SAS treatment in a concentration-dependent form (n = 4). (H, I) The CCK8 assay showed no significant change in cell viability of 661W cells at different SAS concentrations ranging from 0 to 400 μM while SAS combined with H_2O_2 treatment led to decreased cell viability in a dose-dependent manner (n = 5). (J, K) Western blot showing the expression levels of protein Nrf2, GPX4 and HO-1 in 661W cells after treatment of H_2O_2 and SAS (n = 3). Data are shown as mean ± SD. *P < 0.05, **P < 0.01, ****P < 0.0001. All experiments were conducted in triplicate independently. Ctrl: Control; DAPI: 4′,6-diamidino-2-phenylindole; GPX4: glutathione peroxidase 4; HO-1: heme oxygenase-1; NRF2: nuclear factor-erythroid factor 2-related factor 2; ns: not significant; SAS: sulfasalazine; SLC7A11: solute carrier family 7 member 11.

SLC7A11 overexpression suppresses retinal degeneration after light exposure

To explore the therapeutic potential of SLC7A11 overexpression, we injected a recombinant AAV–mediated Slc7a11 vector (rAAV2/8-Slc7a11-GFP) into LIRD mice to deliver an SLC7A11 expression cassette into the photoreceptors. Two weeks later, the mice underwent light exposure. Cryosections revealed efficient transfection of rAAV2/8-Slc7a11-GFP into the retinal pigment epithelium (RPE) and photoreceptors in the whole range of retina (**Figure 7A** and **Additional Figure 8**). We also confirmed the expression of exogenous SLC7A11 and other related proteins including Nrf2, GPX4, HO-1 in the retina by western blotting (**Figure 7B** and **C**). ERG assay before and 3 days after LIRD showed that SLC7A11 overexpression in photoreceptors increased the a-wave (P = 0.0013) and b-wave (P = 0.0039) amplitudes 3 days after LIRD (**Figure 7D** and **E**). We investigated the impact of rAAV2/8-Slc7a11 on photoreceptor cell death and found that SLC7A11 overexpression decreased the numbers of both TUNEL-positive cells (**Figure 7F**) and PI-positive cells (**Figure 7G**) at 3 days after LIRD.

Discussion

Oxidative stress and lipid peroxidation may induce neurodegeneration and photoreceptor loss, contributing to aging and degenerative diseases (Chen et al., 2017; Baksheeva et al., 2018; Zhao et al., 2021a; Gonzalez-Cano et al., 2024). Exposure to visible light induces the release of iron from ferritin, a cytoplasmic protein that stores Fe^{2+}, leading to lipid peroxidation in the outer segments of the photoreceptors (Theriot et al., 2016; Tang et al., 2021b). In this study, we demonstrated that photoreceptors undergo ferroptosis in response to acute light exposure and intense oxidative stress response. SLC7A11, the catalytic subunit of the system xC^-, together with oxidative stress–related proteins Nrf2 and HO-1 were upregulated in the photoreceptors of LIRD mice and H_2O_2-treated 661W cells. Overexpression of SLC7A11 protected the photoreceptors against oxidative stress and ferroptosis by regulating Nrf2, HO-1, and GPX4 proteins. Moreover, SLC7A11 knockdown downregulated the above protective factors, thus aggravating photoreceptor cell damage and ferroptosis both *in vitro* and *in vivo*. The results of this study demonstrated that SLC7A11 overexpression suppressed retinal degeneration in LIRD mice and identified SLC7A11 a potential target for therapy to mitigate damage caused by lipid peroxidation.

Ferroptosis was first identified as a novel form of non-apoptotic programmed cell death in 2012 (Dixon et al., 2012). Ferroptosis is distinct from apoptosis, pyroptosis, necroptosis, and other programmed cell death pathways because it is characterized by lipid peroxidation and is dependent on the accumulation of iron and lipid ROS, which have been reported in numerous cell death–related diseases (Yang and Stockwell, 2016). While iron is necessary for normal visual function, it has also been linked to a variety of retinal diseases. Iron buildup or overload caused by dysfunctional iron metabolism in patients' retinas and vitreous bodies leads to increased oxidative stress, resulting in some chronic degenerative retinopathy associated with increased iron concentrations, including AMD, retinitis pigmentosa (RP), retinal detachment, and glaucoma (Ashok et al., 2020; Zhao et al., 2021a; Yang et al., 2023; Yao et al., 2023). It has been shown that the expressions of iron-processing genes in

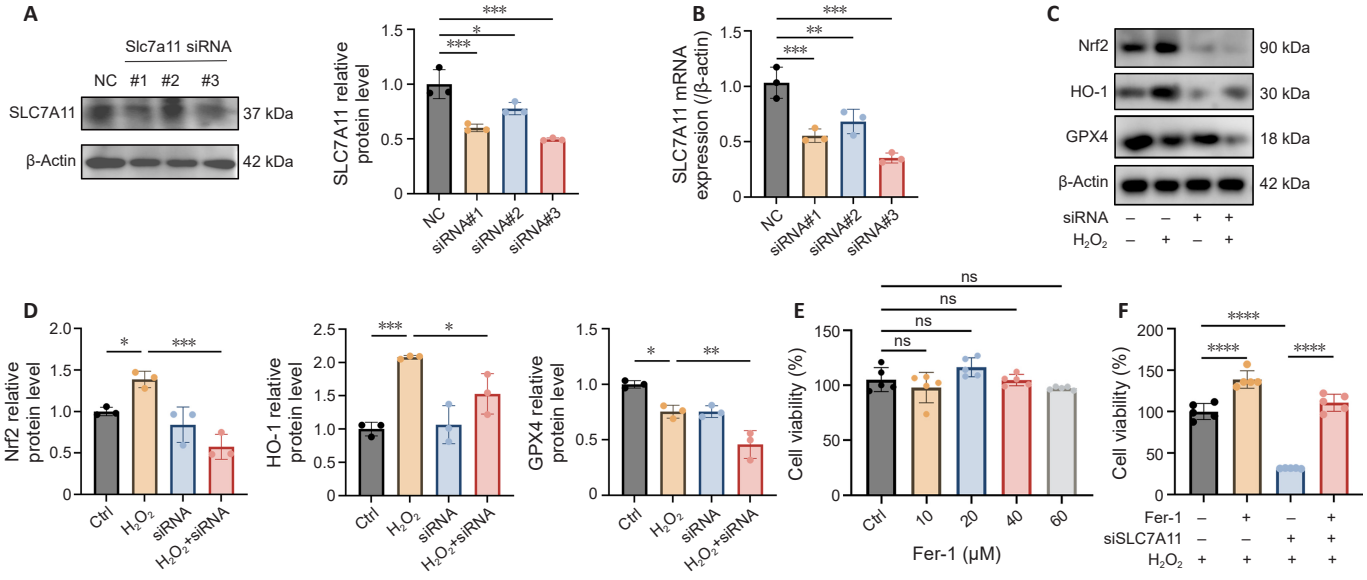

Figure 5 | **SLC7A11 knockdown promotes ferroptosis of 661W cells *in vitro*.**

(A) Western blot analysis of SLC7A11 in 661W cells transfected with various SLC7A11-siRNAs. (B) SLC7A11 mRNA levels in 661W cells transfected with various SLC7A11-siRNAs (n = 3). (C, D) Western blot and data quantification of the expression levels of Nrf2, HO-1, and GPX4 in siSLC7A11#3-treated 661W cells exposed to H_2O_2 (n = 3). (E) CCK-8 assay revealed no significant change in cell viability in 661W cells after treatment with Fer-1 at different concentrations (n = 5). (F) siSLC7A11 transfection significantly decreased the viability of cells treated with 40 μM Fer-1 and H_2O_2 (n = 5). Data are shown as mean ± SD. ns, non-significant. *P < 0.05, **P < 0.01, ***P < 0.001, ****P < 0.0001. All experiments were conducted in triplicate. Ctrl: Control; Fer-1: ferrostatin-1 (ferroptosis inhibitor); GPX4: glutathione peroxidase 4; HO-1: heme oxygenase-1; Nrf2: nuclear factor-erythroid factor 2-related factor 2; ns: not significant; SLC7A11: solute carrier family 7 member 11.

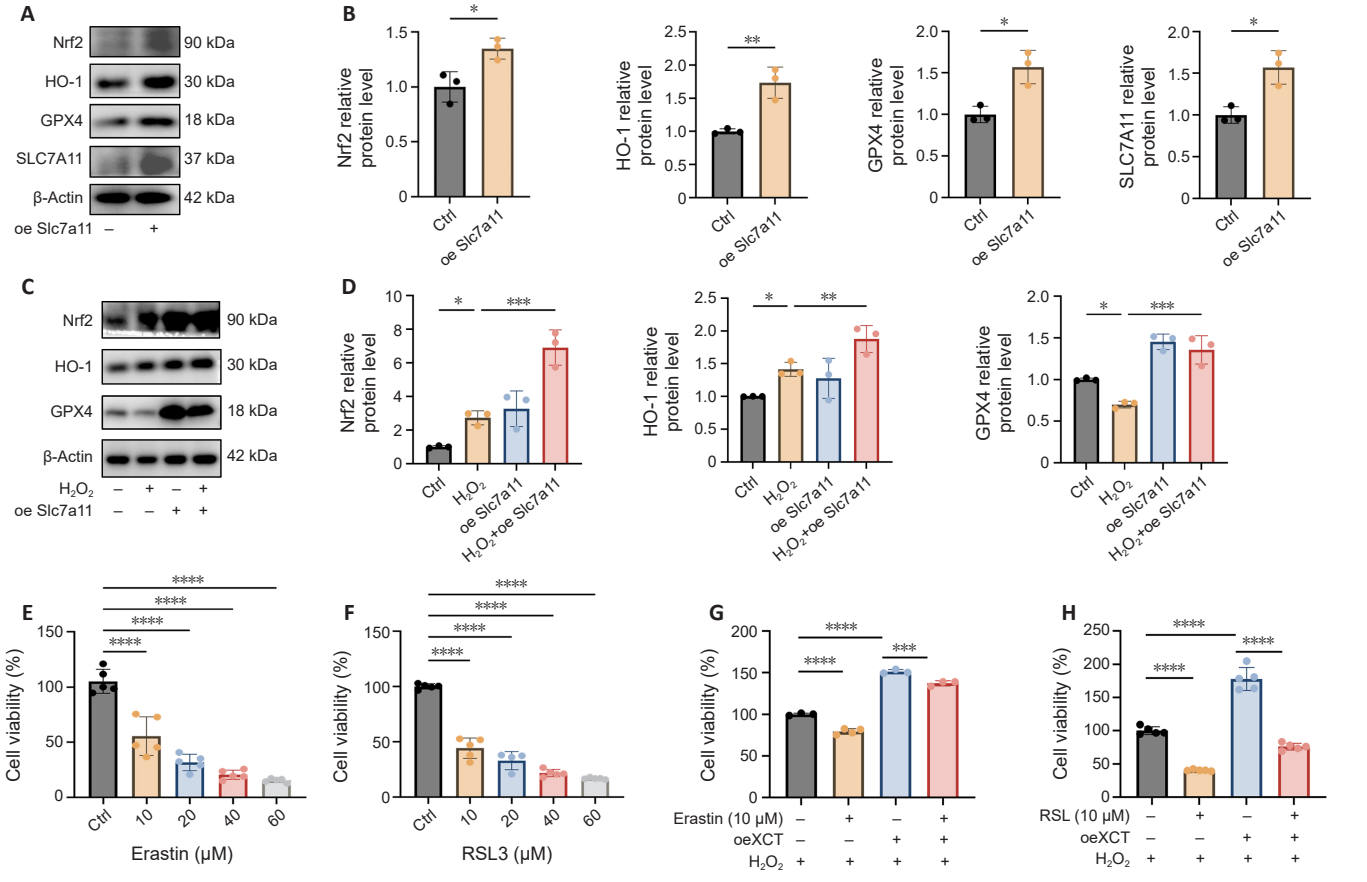

Figure 6 | **SLC7A11 overexpression enhanced ferroptosis resistance *in vitro*.**

(A–D) Western blot of Nrf2, HO-1, SLC7A11, and GPX4 in 661W cells transfected with Slc7a11 plasmid and treated with or without 400 μM H_2O_2 (n = 3). (E, F) Cell Counting Kit-8 assay revealed a significant decrease in cell viability in 661W cells after treatment of Erastin (ferroptosis inducer) or RSL3 (ferroptosis inducer) in a concentration-dependent manner (n = 5). (G, H) SLC7A11 overexpression rescued the cell viability of 10 μM Erastin– or 10 μM RSL3–treated 661W cells after exposure to H_2O_2 (n = 5). Data are shown as mean ± SD. *P < 0.05, **P < 0.01, ***P < 0.001, ****P < 0.0001. All experiments were conducted in triplicate. Ctrl: Control; GPX4: glutathione peroxidase 4; HO-1: heme oxygenase-1; NRF2: nuclear factor-erythroid factor 2-related factor 2; SLC7A11: solute carrier family 7 member 11.

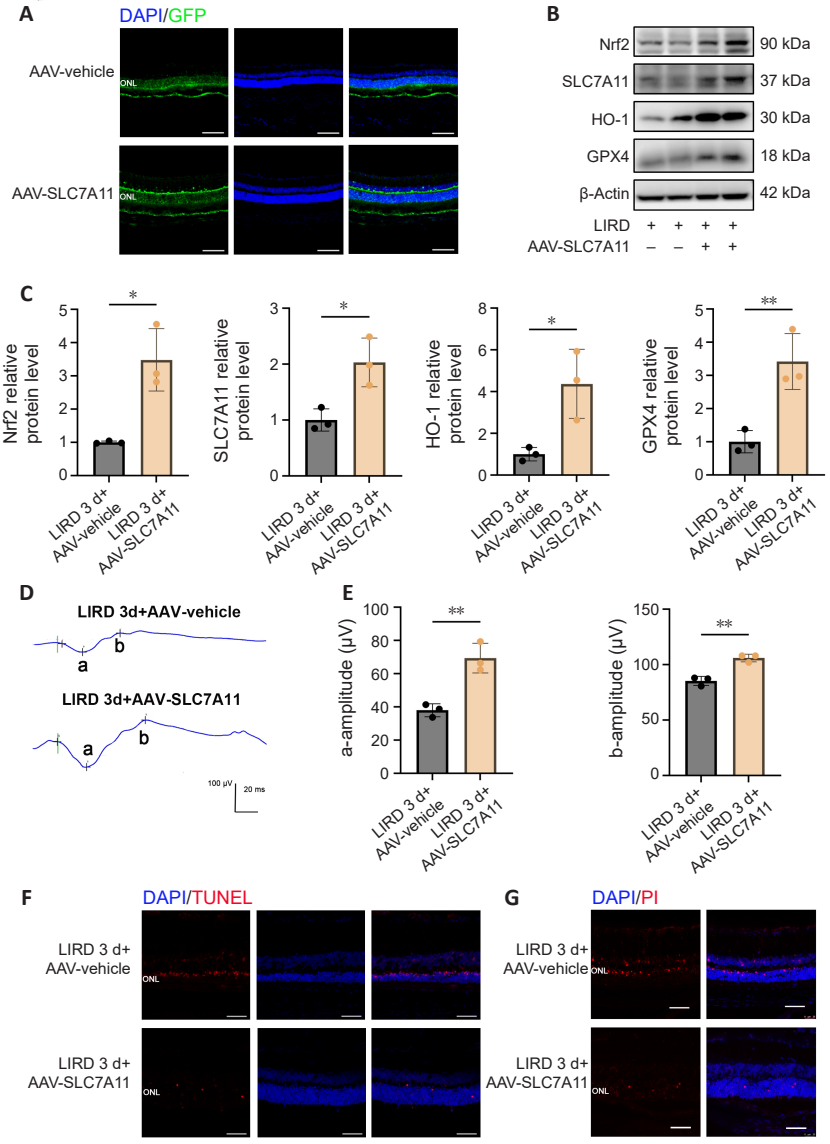

Figure 7 | SLC7A11 overexpression in photoreceptors suppresses retinal degeneration of LIRD mice.

(A) Immunofluorescence of the retinal sections after subretinal injection of AAV2/8-Slc7a11-GFP or AAV2/8-vehicle-GFP for 2 weeks showed AAV transfection reached the photoreceptors. Scale bars: 50 μm. (B, C) Protein expression levels of Nrf2, HO-1, SLC7A11, and GPX4 in retina after LIRD pretreatment with the transfection of AAV2/8-Slc7a11 or AAV2/8-vehicle (n = 3). (D, E) Both the a-wave and b-wave of ERG recordings from mice with 3-day LIRD were increased after AAV2/8-Slc7a11 transfection (n = 3). (F, G) TUNEL (red) and PI (red) staining of retinal sections showed transfection of AAV2/8-Slc7a11 reduced the cell death of photoreceptors caused by light exposure. Scale bars: 50 μm. Data in C and E are shown as mean ± SD. *P < 0.05, **P < 0.01. All experiments were conducted in triplicate. AAV: Adeno-associated virus; DAPI: 4′,6-diamidino-2-phenylindole; GFP: green fluorescent protein; GPX4: glutathione peroxidase 4; HO-1: heme oxygenase-1; LIRD: light-induced retinal damage; NRF2: nuclear factor-erythroid factor 2-related factor 2; SLC7A11: solute carrier family 7 member 11.

the retina greatly change as a result of light exposure. As transferrin receptor levels increase, elevated intracellular iron levels cause excessive oxidative stress (Hadziahmetovic et al., 2012). Photoreceptor degeneration was highly correlated with iron levels in the retinas of light-treated zebrafish (Boyd and Hyde, 2022). Light-exposed photoreceptor cell viability was significantly reduced *in vitro*, which also resulted in ferroptosis-related changes such as iron accumulation, GSH depletion, and decreased GPX4 protein expression (Tang et al., 2021b). Furthermore, the administration of an iron chelator, a well-known ferroptosis inhibitor, showed protective effects in various retinal degenerative models, including the LIRD model (Song et al., 2012; Zhao et al., 2014; Picard et al., 2015). These therapies decrease retinal oxidative stress and increase photoreceptor survival, resulting in both functional and structural rescue. The role of ferroptosis during photoreceptor survival, particularly in retinal degenerative diseases, and the role of SLC7A11 in the regulation of ferroptosis as well as oxidative stress during this process has remained poorly understood. Our study fills the gap in this field by providing potential mechanisms.

SLC7A11, commonly known as xCT, is the major component of the xC^- system, which transports cysteine into cells to reduce cell peroxidation. The ferroptosis inducer erastin inhibits xC^- system activity in cancer cells, causing iron toxicity and inducing SLC7A11 transcription as a compensatory response. Several oncological investigations have revealed that SLC7A11 inhibition is closely associated with ferroptosis (Koppula et al., 2021; Liu et al., 2022; Shen et al., 2022). Therefore, we examined the involvement of SLC7A11 in photoreceptor degeneration. Microarray analysis in a model of photodamage in albino rodents revealed that photic damage caused increased SLC7A11 expression. The retinas of albino mice lack melanin and are more sensitive to light damage. Therefore, we next used C57BL/6 mice with melanin deposition that more closely resemble the normal human physiopathological state and established a stable LIRD mouse model (Zhang et al., 2022). SLC7A11 expression in the retina increased after light damage and peaked 1 day after LIRD. Our *in vitro* investigations showed increased SLC7A11 levels with increasing H_2O_2 concentration and incubation in 661W cells. Therefore, we hypothesized that 661W cells overexpress defense molecules, such as SLC7A11, to compensate for the damage caused by oxidative stress.

Light damage causes photoreceptor cell loss and Fe^{2+} accumulation in the retina, as well as increased ROS levels and lipid peroxidation. Iron overload generates ROS via the Fenton reaction and induces ferroptosis via lipid peroxidation driven by ROS. In addition to SLC7A11, numerous molecules associated with oxidative stress and ferroptosis, including Nrf2, HO-1, and GPX4, were dramatically altered 1 day after exposure to light or 24 hours after H_2O_2 treatment. These findings were validated using *in vitro* and *in vivo* models generated by $NaIO_3$, indicating that oxidative stress causes lipid peroxidation and thereby ferroptosis.

Next, we explored the protective mechanism of SLC7A11 in photoreceptors. SAS is a verified selective SLC7A11 inhibitor. After treatment with SAS, the number of TUNEL-positive cells decreased and the levels of Nrf2, HO-1, and GPX4 decreased after light damage. We observed decreased cell viability and Nrf2, HO-1, and GPX4 expression levels following SAS treatment *in vitro*. Reduced GSH levels and the corresponding decreases in levels of the rate-

limiting enzymes GS and GR associated with GSH synthesis were also detected after SAS treatment. This result is consistent with the previous findings that inhibition of SLC7A11 leads to the deficiency of GS and GR, which inhibits GSH synthesis and subsequent elevated levels of oxidative stress, ultimately leading to ferroptosis (Zhang et al., 2023; Zhu et al., 2023). To further validate the role of SLC7A11 in photoreceptor cells, we used SLC7A11 siRNA and SLC7A11 overexpression plasmids. Following SLC7A11 knockdown, GSH synthesis was stopped; GPX4 could not eliminate lipid peroxides, and ferroptotic cell death commenced. SLC7A11 overexpression led to the opposite results. The ferroptosis inhibitor Fer-1 reduced the siSLC7A11-induced increased mortality of 661W cells by blocking ROS generation and lipid peroxidation compared with H_2O_2 treatment alone. Treatment of 661W cells overexpressing SLC7A11 with the ferroptosis inducers erastin and RSL3 resulted in significantly reduced cell viability, presumably from increased ROS production and lipid peroxidation. The results of our study underscore the therapeutic possibilities of *in vivo* upregulation of SLC7A11 as a means to target ferroptosis. These findings are consistent with those of our previous work showing that SLC7A11 may help prevent choroidal neovascularization by suppressing ferroptosis and protecting against oxidative stress (Zhao et al., 2021b). Hence, SLC7A11 overexpression may represent a therapeutic approach to help treat retinal degenerative diseases including AMD and RP by inhibiting ferroptosis.

The Nrf2 pathway is the main pathway activated in response to oxidative stress. Activated Nrf2 shields cells against damage caused by hydroperoxides (Jaganjac et al., 2020). While Nrf2 activation has long been associated with protection against cell death, the function of Nrf2 in ferroptotic cell death and its relationship with iron signaling is currently in the preliminary stage of investigation (Dodson et al., 2019). While Nrf2 has been shown to upregulate SLC7A11 and GPX4 transcription (Kerins and Ooi, 2018), our results showed that SLC7A11 also affected Nrf2 expression. An siRNA against SLC7A11 demonstrated a similar decrease in Nrf2. In contrast, SLC7A11 overexpression increased Nrf2 expression compared with controls. We speculate that oxidative stress may be prevented by positive feedback regulation between Nrf2 and SLC7A11. However, a clear understanding of the precise processes through which SLC7A11 influences Nrf2 is lacking, and further investigation is required.

In the current study, we found that ferroptosis plays a significant role in light-induced photoreceptor cell death. Nevertheless, photoreceptor degeneration is a complicated pathological process, and ferroptosis is not the sole factor in this process. In addition to the classical apoptotic pathway, autophagy plays a role in photoreceptor cell degeneration (Zhang et al., 2014). Other related investigations have shown a close association between ferroptosis and autophagy, in which autophagy promotes ferroptosis through ferrotinophagy, a type of cargo-specific autophagy (Kong et al., 2019; Tang et al., 2021a). Autophagy is strongly induced by oxidative stress and lipid peroxidation products, and excessive autophagy promotes ferroptosis. SLC7A11 or GPX4 knockdown reduces autophagy, thereby promoting ferroptosis (Alborzinia et al., 2018). Thus, further research on the mechanism underlying the interaction between ferroptosis and autophagy in photoreceptor degeneration is warranted.

This study has several limitations. First, while the 661W cell line is a convenient tool to study photoreceptor cells *in vitro*, it cannot fully simulate *in vivo* states and physiology. Second, we knocked down and overexpressed SLC7A11 to investigate its protective effect. However, it is necessary to further clarify the exact mechanisms involved in this model using SLC7A11 knockout mice, gene editing techniques, and selective receptor agonists/antagonists.

In summary, SLC7A11 plays a critical role in mitigating ferroptosis in light-induced photoreceptor degeneration, the mechanism of which may depend on inhibition of the oxidative stress pathway. Thus, SLC7A11 may be a potential therapeutic target for patients with retinal degenerative diseases. Future studies should focus on the exact mechanisms of action of SLC7A11 in ferroptosis and its function in retinal degenerative diseases.

Acknowledgments: *The authors are grateful to Prof. Guotong Xu (Department of Ophthalmology of Tongji Hospital, Tongji University School of Medicine, Shanghai, China) for providing the murine photoreceptor-derived cell line 661W.*

Author contributions: *XH, YZ, YJ, XZ and JS contributed to the conception and design of the experiments and were responsible for data collection, analysis and interpretation. XH contributed to methodology, investigation, and data curation. XH and JS drafted the manuscript. YZ, YJ, XZ, XS, TL, SY, YW, BY, MZ and GZ conducted data analysis and revised the article critically for important intellectual content. JS and XS provided funding support. JS and XZ are guarantors of this work, who have full access to all the data in this study and take responsibility for the integrity and accuracy of the data. All authors approved the final version of the manuscript for submission.*

Conflicts of interest: *There are no conflicts of interest to disclose.*

Data availability statement: *All relevant data are within the paper and its Additional files.*

Additional files:

Additional Figure 1: *Schematic diagram of the experimental design and timeline for animal and cell experiments.*

Additional Figure 2: *Nuclei rows in the ONL of mice treated with LIRD.*

Additional Figure 3: *Localization of SLC7A11 in photoreceptor cells.*

Additional Figure 4: *MDA levels of 661W cells treated with H_2O_2.*

Additional Figure 5: *The protein expressions of GS and GR in 661W cells treated with SAS.*

Additional Figure 6: *The expressions of NRF2, HO-1, SLC7A11, and GPX4 in 661W cells treated with H_2O_2 or $NaIO_3$.*

Additional Figure 7: *Transfection efficiency of Cy3-siRNA in 661W cells.*

Additional Figure 8: *Transfection range of AAV2/8-SLC7A11 in mouse eyeball.*

Additional Table 1: *Sequences for primers, siRNA, and AAV.*

Additional Table 2: *Primary and secondary antibodies used in western blotting.*

References

Alborzinia H, Ignashkova TI, Dejure FR, Gendarme M, Theobald J, Wölfl S, Lindemann RK, Reiling JH (2018) Golgi stress mediates redox imbalance and ferroptosis in human cells. Commun Biol 1:210.

Ashok A, Singh N, Chaudhary S, Bellamkonda V, Kritikos AE, Wise AS, Rana N, McDonald D, Ayyagari R (2020) Retinal degeneration and Alzheimer's disease: an evolving link. Int J Mol Sci 21:7290.

Baksheeva VE, Tiulina VV, Tikhomirova NK, Gancharova OS, Komarov SV, Philippov PP, Zamyatnin AA Jr, Senin II, Zernii EY (2018) Suppression of light-induced oxidative stress in the retina by mitochondria-targeted antioxidant. Antioxidants (Basel) 8:3.

Blasiak J (2020) Senescence in the pathogenesis of age-related macular degeneration. Cell Mol Life Sci 77:789-805.

Boyd P, Hyde DR (2022) Iron contributes to photoreceptor degeneration and Müller glia proliferation in the zebrafish light-treated retina. Exp Eye Res 216:108947.

Brown EE, DeWeerd AJ, Ildefonso CJ, Lewin AS, Ash JD (2019) Mitochondrial oxidative stress in the retinal pigment epithelium (RPE) led to metabolic dysfunction in both the RPE and retinal photoreceptors. Redox Biol 24:101201

Chan CM, Huang DY, Sekar P, Hsu SH, Lin WW (2019) Reactive oxygen species-dependent mitochondrial dynamics and autophagy confer protective effects in retinal pigment epithelial cells against sodium iodate-induced cell death. J Biomed Sci 26:40.

Chen X, Kang R, Kroemer G, Tang D (2021) Broadening horizons: the role of ferroptosis in cancer. Nat Rev Clin Oncol 18:280-296.

Chen X, Hall H, Simpson JP, Leon-Salas WD, Ready DF, Weake VM (2017) Cytochrome b5 protects photoreceptors from light stress-induced lipid peroxidation and retinal degeneration. NPJ Aging Mech Dis 3:18.

Chow LLC, Mead B (2023) Extracellular vesicles as a potential therapeutic for age-related macular degeneration. Neural Regen Res 18:1876-1880.

Chowers G, Cohen M, Marks-Ohana D, Stika S, Eijzenberg A, Banin E, Obolensky A (2017) Course of sodium iodate-induced retinal degeneration in albino and pigmented mice. Invest Ophthalmol Vis Sci 58:2239-2249.

Deng Y, Qiao L, Du M, Qu C, Wan L, Li J, Huang L (2021) Age-related macular degeneration: Epidemiology, genetics, pathophysiology, diagnosis, and targeted therapy. Genes Dis 9:62-79.

Di Pierdomenico J, Scholz R, Valiente-Soriano FJ, Sánchez-Migallón MC, Vidal-Sanz M, Langmann T, Agudo-Barriuso M, García-Ayuso D, Villegas-Pérez MP (2018) Neuroprotective effects of FGF2 and minocycline in two animal models of inherited retinal degeneration. Invest Ophthalmol Vis Sci 59:4392-4403.

Di Pierdomenico J, Martínez-Vacas A, Hernández-Muñoz D, Gómez-Ramírez AM, Valiente-Soriano FJ, Agudo-Barriuso M, Vidal-Sanz M, Villegas-Pérez MP, García-Ayuso D (2020) Coordinated intervention of microglial and müller cells in light-induced retinal degeneration. Invest Ophthalmol Vis Sci 61:47.

Dixon SJ, Lemberg KM, Lamprecht MR, Skouta R, Zaitsev EM, Gleason CE, Patel DN, Bauer AJ, Cantley AM, Yang WS, Morrison B, 3rd, Stockwell BR (2012) Ferroptosis: an iron-dependent form of nonapoptotic cell death. Cell 149:1060-1072.

Dodson M, Castro-Portuguez R, Zhang DD (2019) NRF2 plays a critical role in mitigating lipid peroxidation and ferroptosis. Redox Biol 23:101107.

Dong H, Qiang Z, Chai D, Peng J, Xia Y, Hu R, Jiang H (2020) Nrf2 inhibits ferroptosis and protects against acute lung injury due to intestinal ischemia reperfusion via regulating SLC7A11 and HO-1. Aging (Albany NY) 12:12943-12959.

Fang X, Cai Z, Wang H, Han D, Cheng Q, Zhang P, Gao F, Yu Y, Song Z, Wu Q, An P, Huang S, Pan J, Chen HZ, Chen J, Linkermann A, Min J, Wang F (2020) Loss of cardiac ferritin H facilitates cardiomyopathy via Slc7a11-mediated ferroptosis. Circ Res 127:486-501.

Gonzalez-Cano SI, Flores G, Guevara J, Morales-Medina JC, Treviño S, Diaz A (2024) Polyoxidovanadates a new therapeutic alternative for neurodegenerative and aging diseases. Neural Regen Res 19:571-577.

Hadziahmetovic M, Kumar U, Song Y, Grieco S, Song D, Li Y, Tobias JW, Dunaief JL (2012) Microarray analysis of murine retinal light damage reveals changes in iron regulatory, complement, and antioxidant genes in the neurosensory retina and isolated RPE. Invest Ophthalmol Vis Sci 53:5231-5241.

Handa JT, Cano M, Wang L, Datta S, Liu T (2017) Lipids, oxidized lipids, oxidation-specific epitopes, and age-related macular degeneration. Biochim Biophys Acta Mol Cell Biol Lipids 1862:430-440.

Jaadane I, Boulenguez P, Chahory S, Carré S, Savoldelli M, Jonet L, Behar-Cohen F, Martinsons C, Torriglia A (2015) Retinal damage induced by commercial light emitting diodes (LEDs). Free Radic Biol Med 84:373-384.

Jaganjac M, Milkovic L, Sunjic SB, Zarkovic N (2020) The NRF2, thioredoxin, and glutathione system in tumorigenesis and anticancer therapies. Antioxidants (Basel) 9:1151.

Kerins MJ, Ooi A (2018) The roles of NRF2 in modulating cellular iron homeostasis. Antioxid Redox Signal 29:1756-1773.

Kim J, Cho K, Choung SY (2020) Protective effect of Prunella vulgaris var. L extract against blue light induced damages in ARPE-19 cells and mouse retina. Free Radic Biol Med 152:622-631.

Kong Z, Liu R, Cheng Y (2019) Artesunate alleviates liver fibrosis by regulating ferroptosis signaling pathway. Biomed Pharmacother 109:2043-2053.

Koppula P, Zhuang L, Gan B (2021) Cystine transporter SLC7A11/xCT in cancer: ferroptosis, nutrient dependency, and cancer therapy. Protein Cell 12:599-620,

Lang X, et al. (2019) Radiotherapy and immunotherapy promote tumoral lipid oxidation and ferroptosis via synergistic repression of SLC7A11. Cancer Discov 9:1673-1685.

Lin JB, Apte RS (2018) NAD(+) and sirtuins in retinal degenerative diseases: A look at future therapies. Prog Retin Eye Res 67:118-129.

Liu L, He J, Sun G, Huang N, Bian Z, Xu C, Zhang Y, Cui Z, Xu W, Sun F, Zhuang C, Man Q, Gu S (2022) The N6-methyladenosine modification enhances ferroptosis resistance through inhibiting SLC7A11 mRNA deadenylation in hepatoblastoma. Clin Transl Med 12:e778.

Madeira MH, Boia R, Santos PF, Ambrósio AF, Santiago AR (2015) Contribution of microglia-mediated neuroinflammation to retinal degenerative diseases. Mediators Inflamm 2015:673090.

Miotto G, Rossetto M, Di Paolo ML, Orian L, Venerando R, Roveri A, Vučković AM, Bosello Travain V, Zaccarin M, Zennaro L, Maiorino M, Toppo S, Ursini F, Cozza G (2020) Insight into the mechanism of ferroptosis inhibition by ferrostatin-1. Redox Biol 28:101328.

Murakami Y, Notomi S, Hisatomi T, Nakazawa T, Ishibashi T, Miller JW, Vavvas DG (2013) Photoreceptor cell death and rescue in retinal detachment and degenerations. Prog Retin Eye Res 37:114-140.

Natoli R, Jiao H, Barnett NL, Fernando N, Valter K, Provis JM, Rutar M (2016) A model of progressive photo-oxidative degeneration and inflammation in the pigmented C57BL/6J mouse retina. Exp Eye Res 147:114-127.

Percie du Sert N, et al. (2020) The ARRIVE guidelines 2.0: Updated guidelines for reporting animal research. PLoS Biol 18:e3000410.

Picard E, Le Rouzic Q, Oudar A, Berdugo M, El Sanharawi M, Andrieu-Soler C, Naud MC, Jonet L, Latour C, Klein C, Galiacy S, Malecaze F, Coppin H, Roth MP, Jeanny JC, Courtois Y, Behar-Cohen F (2015) Targeting iron-mediated retinal degeneration by local delivery of transferrin. Free Radic Biol Med 89:1105-1121.

Pope LE, Dixon SJ (2023) Regulation of ferroptosis by lipid metabolism. Trends Cell Biol 33:1077-1087.

Shen L, Zhang J, Zheng Z, Yang F, Liu S, Wu Y, Chen Y, Xu T, Mao S, Yan Y, Li W, Zhang W, Yao X (2022) PHGDH inhibits ferroptosis and promotes malignant progression by upregulating SLC7A11 in bladder cancer. Int J Biol Sci 18:5459-5474.

Shu W, Baumann BH, Song Y, Liu Y, Wu X, Dunaief JL (2020) Ferrous but not ferric iron sulfate kills photoreceptors and induces photoreceptor-dependent RPE autofluorescence. Redox Biol 34:101469.

Song D, Song Y, Hadziahmetovic M, Zhong Y, Dunaief JL (2012) Systemic administration of the iron chelator deferiprone protects against light-induced photoreceptor degeneration in the mouse retina. Free Radic Biol Med 53:64-71.

Sun Y, Zheng Y, Wang C, Liu Y (2018) Glutathione depletion induces ferroptosis, autophagy, and premature cell senescence in retinal pigment epithelial cells. Cell Death Dis 9:753.

Tang D, Chen X, Kang R, Kroemer G (2021a) Ferroptosis: molecular mechanisms and health implications. Cell Res 31:107-125.

Tang W, Guo J, Liu W, Ma J, Xu G (2021b) Ferrostatin-1 attenuates ferroptosis and protects the retina against light-induced retinal degeneration. Biochem Biophys Res Commun 548:27-34.

Tang Z, Ju Y, Dai X, Ni N, Liu Y, Zhang D, Gao H, Sun H, Zhang J, Gu P (2021c) HO-1-mediated ferroptosis as a target for protection against retinal pigment epithelium degeneration. Redox Biol 43:101971.

Theriot CA, Westby CM, Morgan JLL, Zwart SR, Zanello SB (2016) High dietary iron increases oxidative stress and radiosensitivity in the rat retina and vasculature after exposure to fractionated gamma radiation. NPJ Microgravity 2:16014

Ugarte M, Geraki K, Jeffery G (2018) Aging results in iron accumulations in the non-human primate choroid of the eye without an associated increase in zinc, copper or sulphur. Biometals 31:1061-1073.

Voisin A, Pénaguin A, Gaillard A, Leveziel N (2023) Stem cell therapy in retinal diseases. Neural Regen Res 18:1478-1485.

Wang G, Young SP, Bali D, Hutt J, Li S, Benson J, Koeberl DD (2014) Assessment of toxicity and biodistribution of recombinant AAV8 vector-mediated immunomodulatory gene therapy in mice with Pompe disease. Mol Ther Methods Clin Dev 1:14018.

Wang Y, Zhao X, Gao M, Wan X, Guo Y, Qu Y, Chen Y, Li T, Liu H, Jiang M, Wang F, Sun X (2021) Myosin 1f-mediated activation of microglia contributes to the photoreceptor degeneration in a mouse model of retinal detachment. Cell Death Dis 12:926.

Wu H, Xu J, Du X, Cui J, Zhang T, Chen Y (2020) Shihu Yeguang Pill protects against bright light-induced photoreceptor degeneration in part through suppressing photoreceptor apoptosis. Biomed Pharmacother 126:110050.

Wu J, Gao G, Shi F, Xie H, Yang Q, Liu D, Qu S, Qin H, Zhang C, Xu GT, Liu F, Zhang J (2021) Activated microglia-induced neuroinflammatory cytokines lead to photoreceptor apoptosis in Aβ-injected mice. J Mol Med (Berl) 99:713-728.

Xu W, Tao M, Hu Z, Chang T, Wang Y (2020) Minocycline induces apoptosis of photoreceptor cells by regulating ER stress. Exp Eye Res 190:107887.

Yang M, So KF, Lam WC, Lo ACY (2020) Novel programmed cell death as therapeutic targets in age-related macular degeneration? Int J Mol Sci 21:7279.

Yang WS, Stockwell BR (2016) Ferroptosis: death by lipid peroxidation. Trends Cell Biol 26:165-176.

Yang Y, Wang Y, Deng Y, Lu J, Xiao L, Li J, Zhou Y, Nie F, Chen X, Peng J, Tan H, Qin Y, Peng Q (2023) Fructus Lycii and Salvia miltiorrhiza Bunge extract attenuate oxidative stress-induced photoreceptor ferroptosis in retinitis pigmentosa. Biomed Pharmacother 167:115547.

Yao F, Peng J, Zhang E, Ji D, Gao Z, Tang Y, Yao X, Xia X (2023) Pathologically high intraocular pressure disturbs normal iron homeostasis and leads to retinal ganglion cell ferroptosis in glaucoma. Cell Death Differ 30:69-81.

Zhang K, Gu X, Xia Y, Zhao X, Khoso Pervez A, Li S (2023) MiR-129-3p regulates ferroptosis in the liver of selenium-deficient broilers by targeting SLC7A11. Poult Sci 102:102271.

Zhang TZ, Fan B, Chen X, Wang WJ, Jiao YY, Su GF, Li GY (2014) Suppressing autophagy protects photoreceptor cells from light-induced injury. Biochem Biophys Res Commun 450:966-972.

Zhang Y, Zhao Z, Zhao X, Xie H, Zhang C, Sun X, Zhang J (2022) HMGB2 causes photoreceptor death via down-regulating Nrf2/HO-1 and up-regulating NF-κB/NLRP3 signaling pathways in light-induced retinal degeneration model. Free Radic Biol Med 181:14-28.

Zhao L, Wang C, Song D, Li Y, Song Y, Su G, Dunaief JL (2014) Systemic administration of the antioxidant/iron chelator α-lipoic acid protects against light-induced photoreceptor degeneration in the mouse retina. Invest Ophthalmol Vis Sci 55:5979-5988.

Zhao T, Guo X, Sun Y (2021a) Iron accumulation and lipid peroxidation in the aging retina: implication of ferroptosis in age-related macular degeneration. Aging Dis 12:529-551.

Zhao X, Gao M, Liang J, Chen Y, Wang Y, Wang Y, Xiao Y, Zhao Z, Wan X, Jiang M, Luo X, Wang F, Sun X (2021b) SLC7A11 reduces laser-induced choroidal neovascularization by inhibiting RPE ferroptosis and VEGF production. Front Cell Dev Biol 9:639851.

Zhu H, Cheng Y, Wang X, Yang X, Liu M, Liu J, Liu S, Wang H, Zhang A, Li R, Ye C, Zhang J, Gao J, Fu X, Wu B (2023) Gss deficiency causes age-related fertility impairment via ROS-triggered ferroptosis in the testes of mice. Cell Death Dis 14:845.

Zou M, Ke Q, Nie Q, Qi R, Zhu X, Liu W, Hu X, Sun Q, Fu JL, Tang X, Liu Y, Li DW, Gong L (2022) Inhibition of cGAS-STING by JQ1 alleviates oxidative stress-induced retina inflammation and degeneration. Cell Death Differ 29:1816-1833.

C-Editor: Zhao M; S-Editor: Li CH; L-Editors: Li CH, Song LP; T-Editor: Jia Y

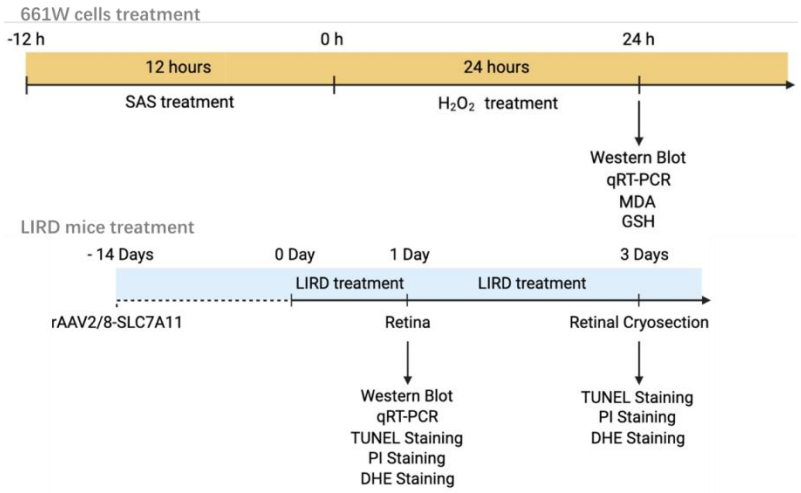

Additional Figure 1 Schematic diagram of the experimental design and timeline for animal and cell experiments.

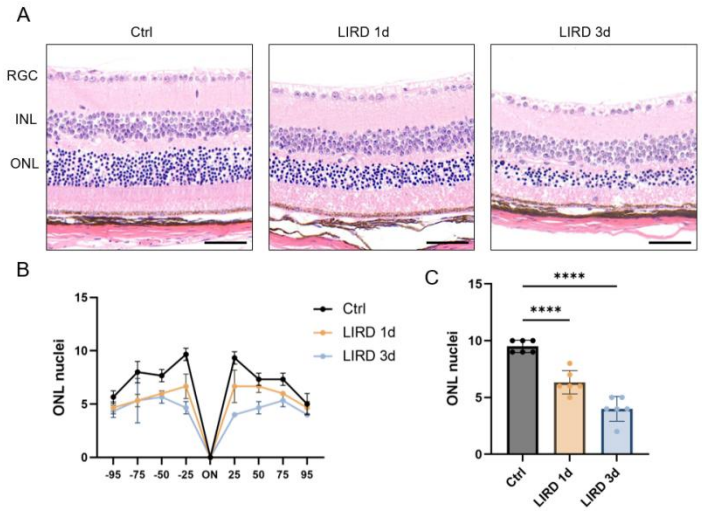

Additional Figure 2 Nuclei rows in the ONL of mice treated with LIRD.

(A) Images of hematoxylin and eosin (H&E)–stained paraffin sections of the control and LIRD-treated group on days 1 and 3. Scale bars: 50 μm. (B) The number of nuclei rows in the ONL at different distances from the optic nerve after 1 and 3 days of LIRD (n = 3). (C) The number of nuclei rows in ONL at 25% distance from the optic nerve after 1 and 3 days of LIRD (n = 6). Data are shown as the mean ± SD. ****P < 0.0001 (one-way analysis of variance with Dunnett's test). Ctrl: control; INL: inner nuclear layer; LIRD: light-induced retinal damage; ONL: outer nuclear layer; RGC: retinal ganglion cell.

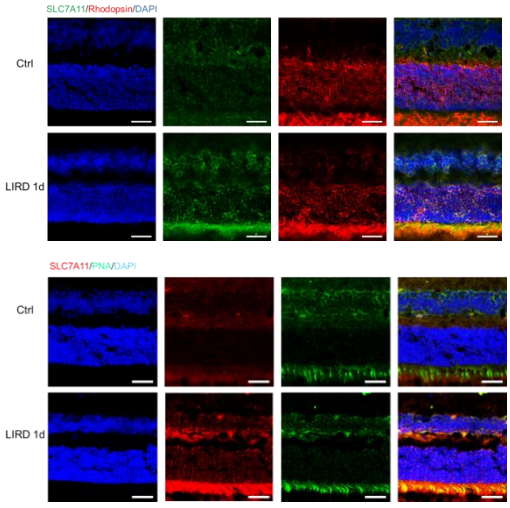

Additional Figure 3 Localization of SLC7A11 in photoreceptor cells.

Immunofluorescence staining of SLC7A11, Rhodopsin (marker for rod), and PNA (marker for cone) in retinal frozen sections before and after LIRD treatment. Scale bars: 25 μm. Ctrl: Control; DAPI: 4',6-diamidino-2-phenylindole; LIRD: light-induced retinal damage; SLC7A11: solute carrier family 7 member 11; PNA: peanut agglutinin.

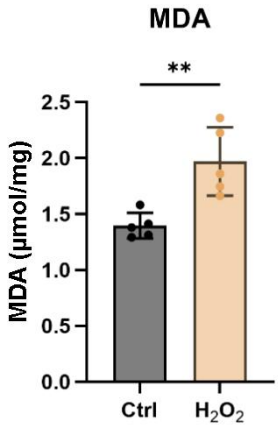

Additional Figure 4. MDA levels of 661W cells treated with H_2O_2.

MDA levels of 661W cells treated with H_2O_2 (n = 5). Data are shown as the mean ± SD; $^{**}P < 0.01$ (Student's t-test). Ctrl: Control; MDA: malondialdehyde.

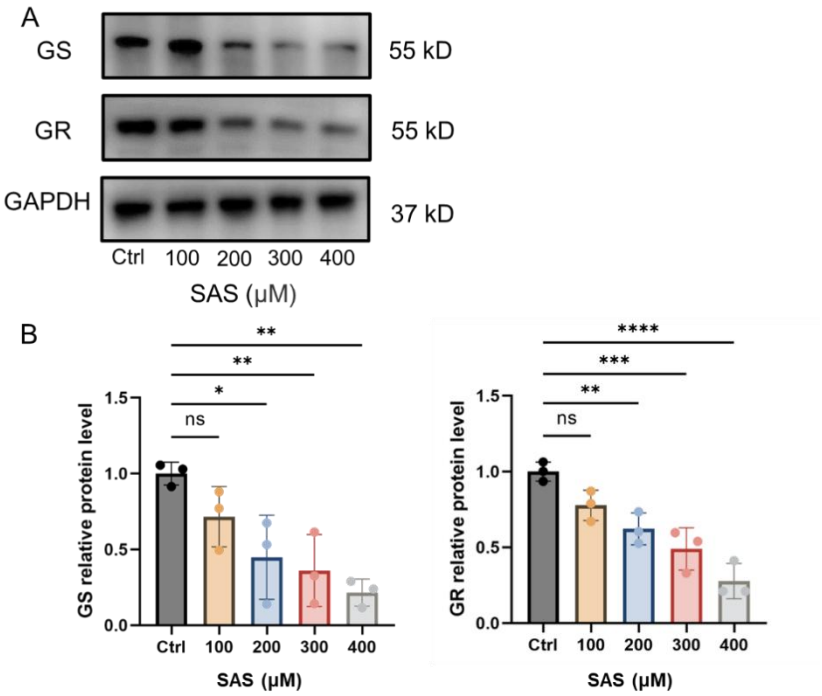

Additional Figure 5 The protein expressions of GS and GR in 661W cells treated with SAS.

(A, B) Western blot analysis and quantification of GS and GR in 661W cells treated with different concentrations of SAS (n = 3). Data in (B) are shown as the mean ± SD. **P* < 0.05, ***P* < 0.01, ****P* < 0.001, *****P* < 0.0001 (one-way analysis of variance with Dunnett's test). GAPDH: Glyceraldehyde-3-phosphate dehydrogenase; GR: glutathione synthase; GS: glutathione reductase; ns: not significant; SAS: SLC7A11 inhibitors sulfasalazine;

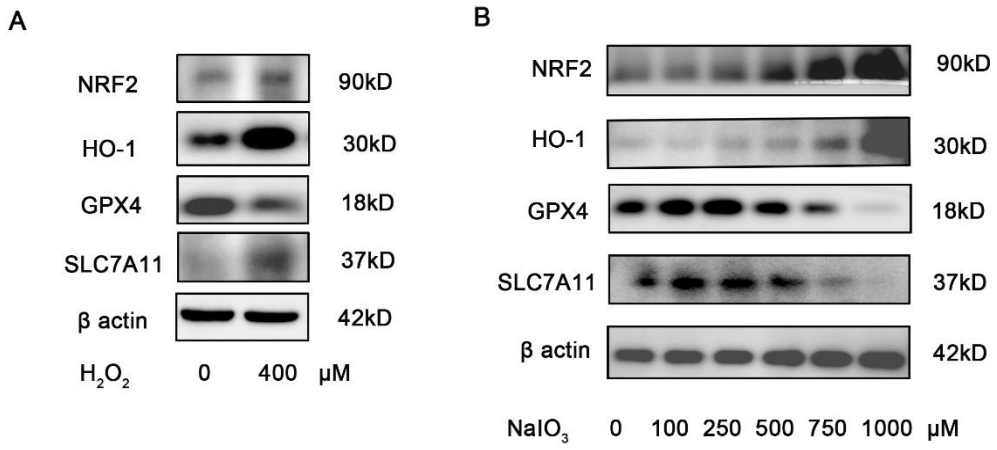

Additional Figure 6 The expressions of NRF2, HO-1, SLC7A11, and GPX4 in 661W cells treated with H_2O_2 or $NaIO_3$.

(A, B) Western blot analysis of NRF2, HO-1, SLC7A11, and GPX4 in 661W cells treated with H_2O_2 (400 μM; A) and different concentrations of $NaIO_3$ for 24 hours (B). GPX4: Glutathione peroxidase 4; HO-1: heme oxygenase-1; NRF2: nuclear factor-erythroid factor 2-related factor 2; SLC7A11: solute carrier family 7 member 11.

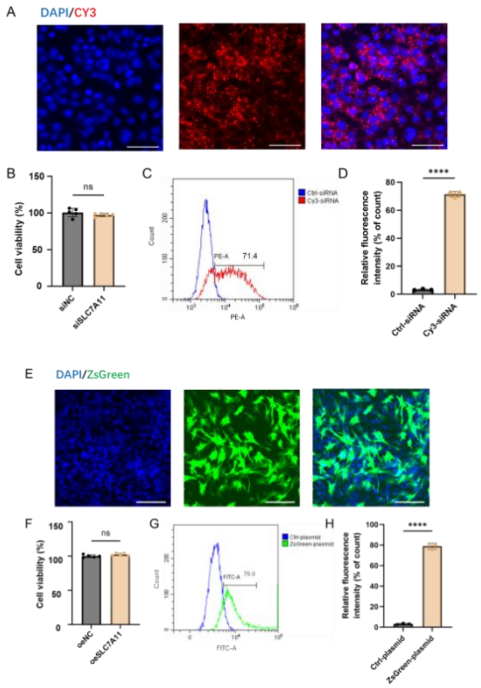

Additional Figure 7 Transfection efficiency of Cy3-siRNA in 661W cells.

(A) Intracellular localization of Cy3-siRNA detected by confocal laser scanning microscopy. (B) Cell viability of 661W cells transfected with siSLC7A11 and siNC (n = 5). (C) Quantitative analysis of the uptake by flow cytometry. (D) Relative fluorescence intensity of Ctrl-siRNA and Cy3-siRNA (n = 3). (E) Intracellular localization of ZsGreen-labeled plasmid detected by confocal laser scanning microscopy. (F) Cell viability of 661W cells transfected with plasmid-NC and plasmid-SLC7A11 (n = 5). (G) Quantitative analysis of the uptake by flow cytometry. (H) Relative fluorescence intensity of Ctrl-plasmid and Zsgreen-plasmid (n = 3). Data in (B, D, F, and H) are shown as the mean ± SD; ****P < 0.0001 (Student's t-test). Scale bars: 50 μm (A), 150 μm (E). Ctrl: Control; DAPI: 4',6-diamidino-2-phenylindole; SLC7A11: solute carrier family 7 member 11.

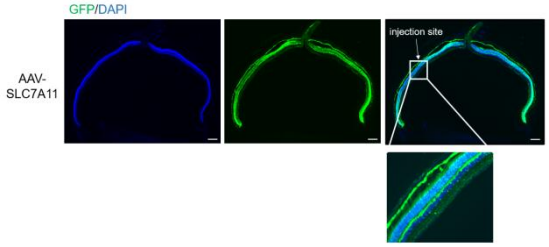

Additional Figure 8 Transfection range of AAV2/8-SLC7A11 in mouse eyeball.

The retinal cryosection after subretinal transfection with AAV2/8-SLC7A11 for 2 weeks. The nuclei were counterstained with DAPI (blue). Scale bars: 200 μm. AAV: Adeno-associated virus; DAPI: 4',6-diamidino-2-phenylindole; GFP: green fluorescent protein; SLC7A11: solute carrier family 7 member 11.

Additional Table 1 Sequences for primers, siRNA, and AAV

siRNA or shRNA	Sequence (5′-3′)
β-actin	F: GGCTGTATTCCCCTCCATCG
	R: CCAGTTGGTAACAATGCCATGT
SLC7A11	F: TGGGTGGAACTGCTCGTAAT
	R: AGGATGTAGCGTCCAAATGC
SLC7A11-si-#1	F: CAACGUUGAUGAUGGACUA tt
	R: UAGUCCAUCAUCAACGUUG tt
SLC7A11-si-#2	F: GAUUUAUCUUCGAUACAAA tt
	R: UUUGUAUCGAAGAUAAAUC tt
SLC7A11-si-#3	F: CCAGAUAUGCAUCGUCCUU tt
	R: AAGGACGAUGCAUAUCUGG tt
siRNA NC	F: UUCUCCGAACGUGUCACGUdTdT
	R: ACGUGACACGUUCGGAGAAdTdT
AAV-SLC7A11	F: TGGGTGGAACTGCTCGTAAT
	R: AGGATGTAGCGTCCAAA TGC

AAV: Adeno-associated virus; **F:** Forward; R: reverse; SLC7A11: solute carrier family 7 member 11.

Additional Table 2 Primary and secondary antibodies used in western blotting

Antibody	Dilution	Cat#	RRID	Supplier
Rabbit anti-SLC7A11	1:1000	12691S	AB_2687474	Cell Signaling Technology, Danvers, MA, USA
Rabbit anti-Nrf2	1:1000	16396-1-AP	AB_2782956	Proteintech, Wuhan, Hubei, China
Rabbit anti-HO-1	1:1000	10701-1-AP	AB_2118685	Proteintech
Rabbit anti-GPX4	1:1000	ab125066	AB_10973901	Abcam, Cambridge, MA, USA
Rabbit anti-GS	1:1000	15712-1-AP	AB_2878171	Proteintech
Rabbit anti-GR	1:1000	18257-1-AP	AB_10598162	Proteintech
Rabbit anti-β-actin	1:1000	20536-1-AP	AB_10700003	Proteintech
Horseradish peroxidase-conjugated Affinipure goat anti-rabbit IgG(H + L)	1:5000	SA00001-2	AB_2722564	Proteintech

GPX4: Glutathione peroxidase 4; GR: glutathione synthase; GS: glutathione reductase; HO-1: heme oxygenase-1; Nrf2: nuclear factor-erythroid factor 2-related factor 2; SLC7A11: solute carrier family 7 member 11; HRP: horseradish peroxidase.